Challenge Journal of Concrete Research Letters

Research Article

Structural behavior of ferrocement composite hollow-cored panels for roof construction

Yousry B. I. Shaheen [a], Zeinab A. Etman [a,b,*], Aya M. Elrefy [b]

[a] *Department of Civil Engineering, Menoufia University, Shebin ElKoum, Menofia, Egypt*
[b] *Department of Civil Engineering, Higher Institute of Engineering and Technology, Menofia, Egypt*

ABSTRACT

The main objective of the following work is to study the effect of using different types of metallic and non-metallic mesh reinforcement materials on the flexural behavior of ferrocement hollow-cored panels as a viable alternative for conventional reinforced concrete roofs. The proposed panels are lighter in weight relative to the conventional reinforced concrete panels. Three types of the steel meshes were used to reinforce the ferrocement skin layers. Namely: welded wire mesh, expanded metal mesh, and tenax mesh with various numbers of layers. Experimental investigation was conducted on the proposed panels. A total of ten slabs having the total dimensions of 2000 mm length, 500 mm width and 120 mm thickness were cast and tested under flexural loadings until failure. The deformation characteristics and cracking behavior were recorded and observed for each panel at all stages of loadings. The results showed that high ultimate and serviceability loads, crack resistance control, high ductility, and good energy absorption properties could be achieved by using the proposed panels. This could be of true construction merits for both developed and developing countries alike. The experimental results were then compared to analytical models using (ABAQUS/Explicit) programs. The finite element (FE) simulations achieved better results in comparison with the experimental results.

ARTICLE INFO

Article history:
Received 13 July 2021
Revised 28 September 2021
Accepted 28 December 2021

Keywords:
Hollow core slab
Ferrocement
Composite materials
Tenax mesh
Experimental program

1. Introduction

A hollow core slab, known as a void slab, hollow core plank or simply a concrete plank is a precast concrete slab typically used in the construction of roofs in multi-story apartment buildings. Precast concrete popularity is linked with low-seismic zones and more economical constructions because of fast building assembly, lower self-weight (less material), etc. The precast hollow core concrete slab has voids extending the full length of the slab which makes the slab much lighter than a massive solid concrete slab of equal thickness or strength. The reduced weight is important because it lowers the costs of transportation as well as material (concrete) costs. Hollow core slabs are most widely known for providing economical, efficient floor and roof systems.

On the other hand, ferrocement is a construction material that proved to yield superior properties in terms of crack control, impact resistance, and toughness, largely due to the close spacing and uniform dispersion of reinforcement within the material. In 1999, the American Concrete Institute ACI committee 549 give the following definition in the state-of-the-art report on ferrocement (ACI 549R) "ferrocement is a type of thin wall reinforced concrete commonly constructed of hydraulic cement mortar reinforced with closely spaced layers of continuous and relatively small size wire mesh. The mesh may be made of metallic or other suitable materials".

A literature review was presented by Koukousel and Mistakid (2014) and Sakthivel and Jagannathan (2005) on ferrocement as a construction material. Ferrocement can be used in different applications due to its properties such as different roofing systems, retaining walls, sculptures, bus shelters, bridge decks, repair works, water structures like tanks, strengthening and precast ferrocement elements (Aboul-Anen et al. 2009; Ali and Abdullah

* *Corresponding author*. Tel.: +2-01-009-727355 ; E-mail address: :zeinab.etman@sh-eng.menofia.edu.eg (Z. A. Etman)
ISSN: 2548-0928 / DOI: https://doi.org/10.20528/cjcrl.2022.01.002

1995; Al-Kubaisy and Jumaat 2000; Elavenil and Chandrasekar 2007; Fahmy et al. 1997). Additionally, ferrocement is lighter than traditional concrete up to 70% elements, which can be suitable for low-cost housing (Leeanansaksiri et al. 2018; Naaman 2015; Shaheen and Eltahawy 2017). The effect of the strength of ferrocement jackets for initially damaged exterior RC beam-column joints is presented by Singh et al. (2015). In this study, the experimental observation noticed an improvement in the ultimate load, yield load carrying capacity with increase in stiffness of the ferrocement-jacketed joints in comparison with the control joint.

Many investigators have reported the advantages of ferrocement in comparing with the conventional reinforced concrete. In addition, numerous test data are available to define its performance criteria for construction and repair of structural elements (Shaheen et al. 2018; Fahmy et al. 2004, 2005). From these investigations, it can be concluded that ferrocement has features included ease of prefabrication and low cost in maintenance and repair. Swamy and Shaheen (1990) investigated the comprehensive test data on the tensile behavior of ferrocement plates, 12.5mm thick. The results showed that the composite properties of elastic modulus and ultimate tensile strength could be very satisfactorily predicted. However, the cracking behavior for a wide range of mesh geometry could not be satisfactorily predicted by a single unique relationship. There was, however, a good correlation between the composite properties of ultimate tensile strength and ultimate flexural strength. The results show that by suitable design of the matrix and the reinforcement, high strength ferrocement sheets with high crack resistance can be developed for a variety of structural applications.

Furthermore, many attempts have been made to improve the practical use of the ferrocement I-beams by developing its ductile behavior. For example, the evaluation of the actual flexural capacity of the ferrocement I-beam with additional layers of wire mesh in the flange section as compared to the theoretical analysis computation is illustrated by Acma et al. (2015). The design and construction of the ferrocement channels were presented with various materials (e.g., meshes and mortar). In addition, an optimal combination of meshes was obtained and finite element FE models of the channels were implemented using ABAQUS Unified FEA (Eskandari and Madadi, 2015). Ferrocement developed sandwich panels for use as wall bearing units, also studied the structural behavior of light weight ferrocement walls. The proposed panels are lighter in weight relative to the conventional reinforced concrete panels (Shaheen et al. 2020; Shaaban et al. 2018).

Bhalsing et al. (2014) studied the tensile strength behavior of ferrocement due to the specific surface area. A relation between the tensile strength of ferrocement and its mechanical properties were determined. Therefore, utilizing ferrocement in hollow core elements can reduce the self-weight of the elements considerably. Furthermore, the hollow core ferrocement elements are generally more ductile when compared with the hollow conventional reinforced concrete units, because of the fact that the reinforcement in ferrocement is uniformly distributed over the entire section of the hollow elements.

Abbas et al. (2020) studied the flexural response of hollow high strength concrete beams considering different size reductions. The test results showed that ductility of hollow beams with size reductions of 16% and 28.4% was higher than that of the reference solid beam, while the ductility of the hollow beam with 44.4% size reduction was quite comparable to that of the solid beam. Naser et al. (2021) applied an experimental investigation to study the effect of using different types of reinforcement on the flexural behavior of ferrocement thin hollow core slabs with embedded PVC pipes. The results showed that the slab reinforced with only macro steel fibers provided the highest flexural strength, while that reinforced with steel bars showed the highest stiffness and lowest deflection among all tested slabs. Prakashan et al. (2016) applied an experimental study on the flexural behavior of hollow core concrete slabs. The results showed that the conventional flexural capacity equation for solid concrete slabs can predict the flexural capacity of hollow core concrete slabs with an accuracy of ± 19%. And the load - deflection behavior and the serviceability performance of hollow core concrete slabs are significantly better than conventional solid concrete slabs.

Shaheen et al. (2016) investigated the behaviour of ferrocement sandwich panels slabs under shear. Their results concluded further that the developed composite ferrocement slabs emphasized better deformation characteristics and higher cracking and ultimate loads. Du et al. (2021) investigated a new mechanical model of polyvinyl alcohol fiber–reinforced ferrocement cementatious composite (PVA-RFCC), which was reinforced with both PVA fiber and steel wire mesh (SWM). A series of experiments were conducted to study their mechanical properties, and a comparative analysis was also performed to evaluate their flexural toughness. In the same vein, Abdul-Fataha (2014) and Shaheen et al. (2014a) employed numerical models and designed an experimental program to investigate the structural behavior ferrocement beams under three point loadings up to failure. The results of the numerical models and experimental tests indicated that the beam with fiberglass meshes gives the lowest first crack load and the maximum load. Shaheen et al. (2014b) estimated the structure performance of ferrocement domes reinforced with composite material. The results of the experimental program indicated that the dome reinforced with fiberglass mesh has the highest service load and ultimate load and the dome reinforced with welded wire meshes achieved highest ductility ratio and energy absorption. Additionally comparing the results of FE simulations with the experimental results showed that the results of FE simulation is closed the experimental results.

Advantages of ferrocement are;

- It can be fabricated into any shape required.
- The material is very dense, but structures made from it are light in weight.
- It is more durable than most woods and more economical than imported steel.
- The basic raw materials for the construction of ferrocement sand, cement, and reinforcing mesh are readily available in most countries.

- Except for highly stressed or critical structures such as deep-water vessels, adequate ferrocement construction does not demand stringent specifications.
- Little new training is required for the laborers, providing a skilled supervisor is on hand.
- Reduction in time and cost.
- Easily repaired.

Disadvantages of ferrocement are;

- Fastening with bolts, screws, nails, and such like, can be difficult on ferrocement.
- The labor-intensive nature of it, which makes it expensive for industrial application in the western world.
- In addition, threats to degradation (rust) of the steel components
- These air voids can turn to pools of water as the cured material absorbs moisture. If the voids occur where there is untreated steel, the steel will rust and expand, causing the system to fail.
- Tying rods and mesh together is time-consuming.

2. Research Signification

The objective of the work presented in this research was to study the influence of several types of metal and non-metal mesh reinforcement materials on the flexural behavior of ferrocement hollow-cored panels as a viable alternative to traditional reinforced concrete panels. Compared with the traditional reinforced concrete part, the weight of the test part is lighter. In order to strengthen these hollow-cored panels, three types of steel mesh, Welded wire mesh, expanded steel wire mesh and tenax mesh with various layers are used. The parameters investigated in this study are:

- Effect of the number of layers of steel reinforcement provided.
- Effect of the type of steel reinforcement used.

An experimental plan was carried out on the test samples. Ten hollow-cored panels with dimensions of 500mm*2000mm*120mm were casted and tested until they failed under flexural load. Record and observe the deformation characteristics and cracking behavior of each sample during the loading process. Experimental results are then compared to analytical models using (ABAQUS/Explicit) programs. According to the results, high ultimate load and serviceability load, crack resistance control, high ductility and strong energy absorption characteristics have been obtained.

This has the chance to be a true construction benefit to developed and poor countries. The test results of the ferrocement hollow-cored panels revealed that using double-layer of expanded steel mesh as the additional reinforcement of the main steel can achieve the best performance of the reinforced concrete hollow-cored panels. The Finite Element (FE) simulations have achieved better results in comparison with the experimental results. Hollow Core Slabs have many applications in residential, social, industrial, commercial and infrastructure construction such as industrial and large commercial roof covering, floors for multistory buildings, used with steel structures and underground car parking.

3. Experimental Program

The experimental program includes the construction and testing of ten hollow-cored panels 2000 mm long 500 mm wide and 120 mm total thickness. The main goal is to investigate the ultimate load, flexural behavior, ductility ratio, energy absorption and mode of failure at collapse of the control panels, which are reinforced with steel bars and, then, to compare their behavior with those ferrocement panels reinforced with welded galvanized steel mesh and expanded metal mesh and tenax mesh. Skeletal steel bars are used with steel and tenax meshes. Five designations series are then developed as shown in Table 1, along with the details of the experimental program of all the test specimens. Fig. 1 also reveals all the details of reinforcement for all specimens.

Table 1. Details of test specimens.

Specimens designation	Code of panels	Reinforcement wire mesh	Reinforcement details		
			Tension steel bars, Ø6 mm	Compression steel bars, Ø6 mm	No. of stirrups, Ø6 mm/m'
A	O1	With fiber	6	6	6
	O2	Without fiber	6	6	6
B	E1	One layer of expanded steel mesh	6	6	------
	E2	Two layers of expanded steel mesh	6	6	------
C	W2	Two layers of welded steel mesh	6	6	------
	W3	Three layers of welded steel mesh	6	6	------
	W4	Four layers of welded steel mesh	4	4	------
D	M1	One layer of expanded steel mesh +one layer of welded steel mesh	6	6	------
E	T1	One layer of tenax LBO SAMP	6	6	------
	T2	Two layers of tenax LBO SAMP	6	6	------

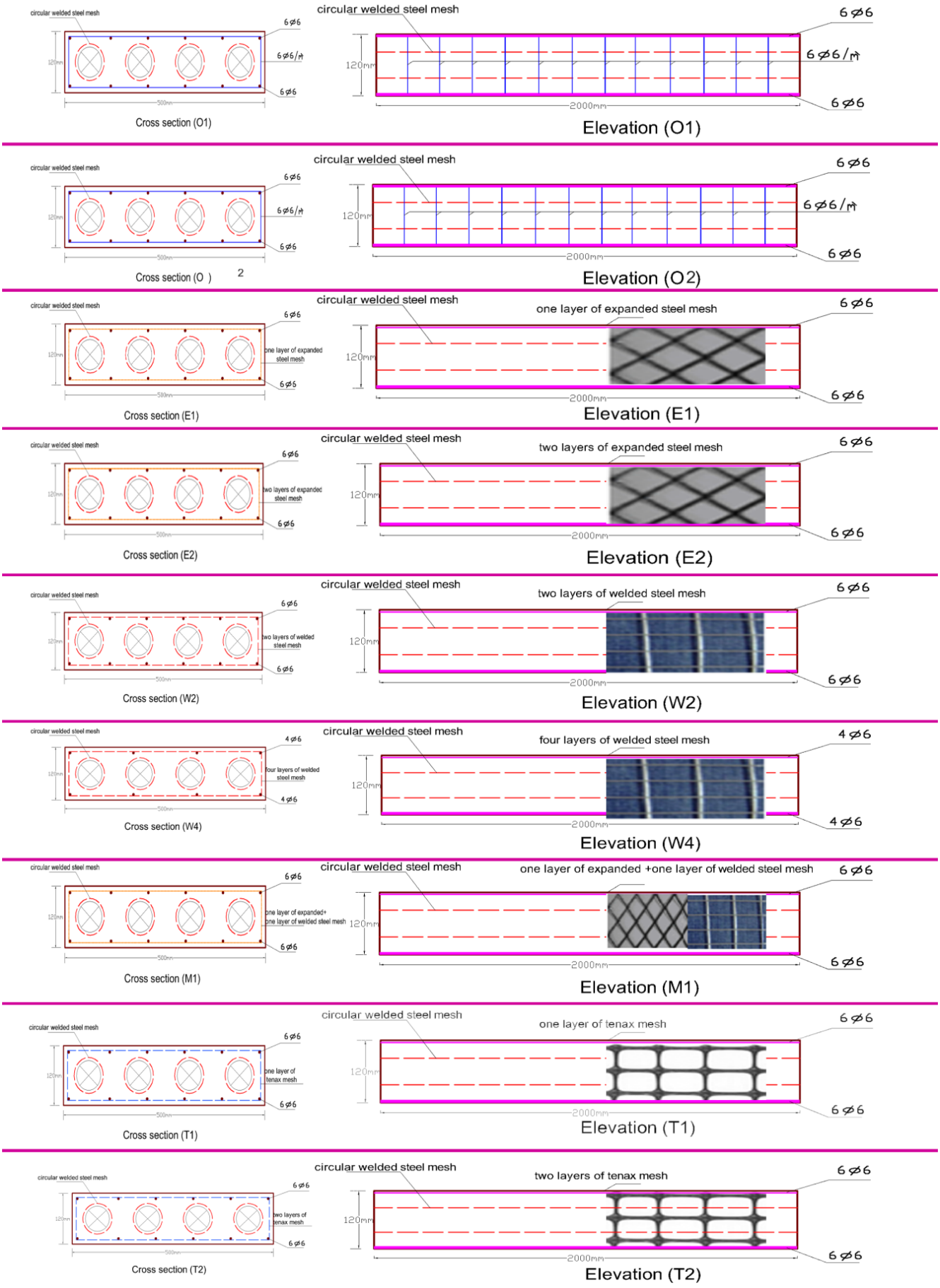

Fig. 1. Reinforcement details of the tested specimens.

3.1. Material properties

• The fine aggregate used in the study is natural siliceous sand. It is clean and nearly free from impurities with a specific gravity of 2.66 and a volume weight of 1.588 t/m^3. Its characteristics satisfy the requirements of the Egyptian Code of Practice (E.C.P. 203/2018) and Egyptian Standard Specifications (E.S.S. 1109/2008).
• The cement used is ordinary Portland cement (CEM I, 42.5 N) (LAFARGE cement). It is physical and chemical properties meeting the requirements of the Egyptian Standard Specifications (E.S.S. 4756-1/2013) as shown.
• Silica fume (S.F) was employed in the present work to increase the strength and permeability of the mortar matrix. It was used as partial replacement by weight of cement in the mortar mixtures. The S.F. had an average particle size of 0.1 micrometer and a silicon dioxide content of 93%.
• Fly ash is a concrete additive of a new generation in fine powder form and spherical particles which reduces the water requirements and creates a lubricating effect that causes concrete to flow and pump better. In addition the concrete is more cohesive and is less prone to segregation. Fly ash had a relatively low specific gravity of 2.20.
• Polypropylene fibres mesh e-300: Using only 100% virgin homopolymer polypropylene graded fibrillated fibers containing no reprocessed olefin components that meets ASTM C-1116, A minimum of 900 grammes (0.9kg/m^3) of application per cubic metre is required. Fibers are commonly utilised to prevent cracking caused by drying shrinkage and thermal expansion/contraction. It was also utilised to reduce permeability in concrete, improve impact capacity, shatter resistance, and abrasion resistance, as well as add fibrillated toughness and residual strength. The technical specifications and mechanical properties of Polypropylene fibres e-300 as provided by producing company are given in Table 2, shown in Fig. 2.
• The water used was clean drinkable water, free from impurities was used for mixing and curing processes. The properties of the used water achieve the Egyptian Code of Practice (E.C.P. 203/2018) requirements.
• Super plasticizer used was a high rang water reducer HRWR. It was used to improve the workability of the mix. The admixture used was produced by CMB GROUP under the commercial name of Addicrete BVF. It meets the requirements of ASTM C494 (type A and F) (Singh et al., 1986). The admixture is a brown liquid having a density of 1.18 kg/liter at room temperature. The amount of HRWR was 1.0% of the cement weight.
• Reinforcing steel: Normal mild steel bars were used, produced from the Ezz Al Dekhila Steel - Alexandria Its chemical and physical characteristics satisfy the Egyptian Standard Specification E.S.S. 262/2011. Mild steel bars of 6 mm diameter were used with yield strength of 240 MPa.
• Reinforcing meshes
- Expanded steel mesh is used as reinforcement for ferrocement girders. The technical specifications and mechanical properties of expanded metal mesh as provided by producing company are given in Table 3 and shown in Fig. 2.
-Welded metal mesh used was obtained from China, and it was used as reinforcement for ferrocement panels. The technical specifications and mechanical properties of welded steel mesh as provided by producing company are given in Table 3. It is complying with of ACI 549.1R-97 (2009) shown in Fig. 2.
-Tenax LBO SAMP (330) is polypropylene Geogrid especially for reinforcement applications. The geogrid is manufactured from a unique process of extrusion and biaxial orientation to enhance their tensile properties. It features consistently high tensile strength and modulus, excellent resistance to construction damages and environmental exposure. Properties of this mesh can be shown in Table 3 and Fig. 2.

Table 2. Chemical and physical properties of fiber mesh e-300.

Fiber Length	Type / Shape	Absorption	Specific Gravity	Electrical Conductivity	Acid & Salt Resistance	Melt Point	Ignition Point	Thermal Conductivity	Alkali Resistance
Various	Graded / Fibrillated	Nil	0.91	Low	High	162°C (324°F)	593°C (1100°F)	Low	Alkali Proof

Table 3. Technical specifications and mechanical properties of expanded metal, welded metal and tenax meshes.

Expanded Metal Mesh		Welded Metal Mesh		Tenax LBO 330	
Style	1532	Dimensions	12.5mm × 12.5mm	Structure	Biaxial geogrid
Sheet Size	1m × 10m	Weight	430 g/m^2	Mesh type	Rectangular apertures
Weight	1.3 kg/m^2	Proof Stress	400 N/mm^2	Standard colour	Black
Diamond size	16mm × 31mm	Ultimate Strain	$58.8 \cdot 10^{-3}$	Polymer type	Polypropylene
Dimensions of strand	1.25 × 1.5mm	Proof Strain	$1.17 \cdot 10^{-3}$	Carbon black content	2%
Proof Stress	199 N/mm^2	Ultimate Strength	600 N/mm^2	Dimensional characteristics	(LBO 330) Samp
Proof Strain	$9.7 \cdot 10^{-3}$			Aperture size MD	40 mm
Ultimate Strength	320 N/mm^2			Aperture size TD	27 mm
Ultimate Strain	$59.2 \cdot 10^{-3}$			Mass per unit area	420 g/m^2

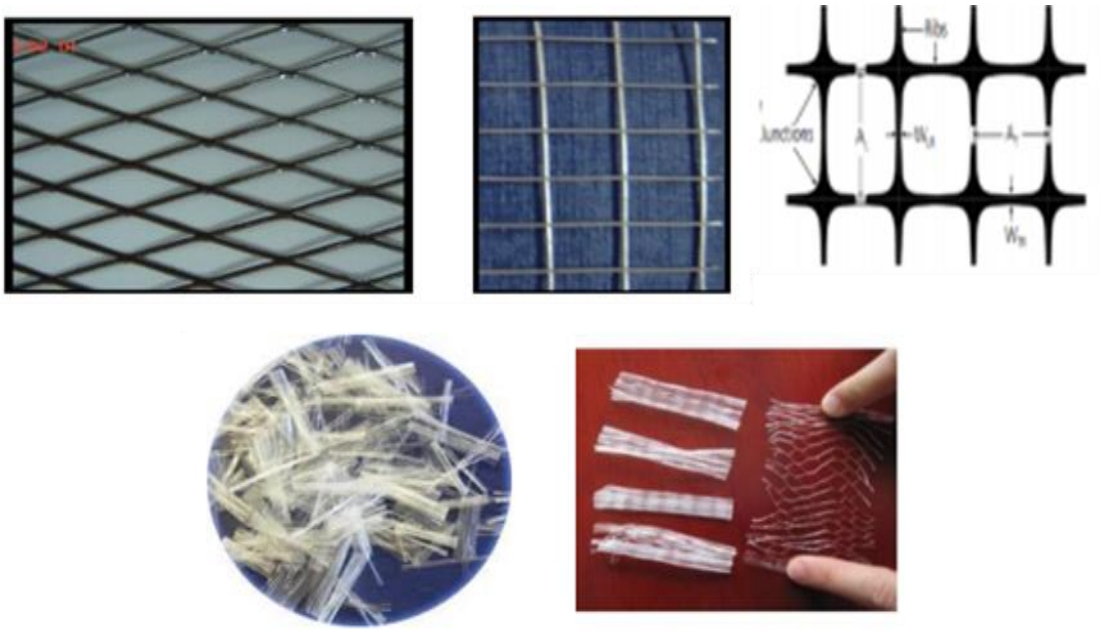

Fig. 2. Types of meshes and fiber e-300.

3.2. Mortar matrix

The sand-cement mortar of ferrocement consisted of sand, ordinary Portland cement, silica fume and fly ash. The main purpose of mix design was to determine how the high amount of cement could be partially replaced by silica fume and fly ash to increase strength of mortar matrix with no detrimental effects on the quality and properties of the mix in both the fresh and hardened states. The requirement of good workability was essential, to allow the mortar matrix to penetrate through the layers of steel mesh reinforcement. A super plasticizing agent was used to increase flow characteristics and accelerate the early strength development. Mortar mixtures for the ferrocement were made using a water / cement ratio of 0.35, super-plasticizer of 2% by weight of cement, while sand/cement ratio of 2.0, 10% by weight of cement was replaced by S.F and 20% by weight of cement was replaced by fly ash and the percentage of addition of fiber e-300 was chosen as 0.9 kg/m^3. The average compressive strength of the ferrocement mortar after 28 days, (fcu), was found to be 35 MPa. For all mixes, mechanical mixer in the laboratory used mechanical mixing with capacity of 0.05 m^3, where the volume of the mixed materials was found to be within this range. The constituent materials were first dry mixed; the mix water was added and the whole patch was re-mixed again in the mixer. The mechanical compaction was applied for all specimens.

3.3. Preparation of test specimens

The mold from rectangular forms from contras wood with entire size of 500x120x2000 mm was prepared and used for casting panels. The pipes from plastic with diameter 50 mm and 2200 mm length were prepared and used to keep the required voids. The ferrocement forms were left for 24 hours in the mold before disassembling the mold. Lastly, the forms were covered with wet burlap for 28 days. All of previous steps are shown in Fig. 3.

3.4. Test setup

At the time of testing, the specimen was painted with white paint to facilitate the visual crack detection during testing process. A set of four "demec" points was placed on one side of the specimen to allow measuring the strain versus load during the test. Demec points were placed as shown in Fig. 4. The specimens were tested on a testing loading frame with a four loading points. The span length was 1800 mm while the distance between the two loading points was 600 mm. dial gauges were used to measure deflection at mid span and under points of loading while strain gauges attached to the top and bottom of the surface of concrete at the critical sections to evaluate its behavior. All the values of deflection at the variable positions and top and bottom strain values were recorded. Cracks were traced throughout bottom of the specimen and then marked with black markers. The first crack-load of each specimen was recorded. The load was increased until complete failure of the specimen was reached. Test setup of specimen can be shown in Fig. 5.

4. Experimental Results and Discussions

The obtained results for the first cracking load, ultimate load, Serviceability Load, ductility ratio and energy absorption as shown in Table 4, Ultimate load and deflection at ultimate load were measured and obtained during the test, while ductility ratio, serviceability load and energy absorption were determined from the load–deflection diagram for each tested panel. Fig. 6 represents the values for the first cracking load and ultimate load for all the tested panels. Maximum ultimate load reached 50 kN for E2 and minimum ultimate load achieved 32 kN.

Fig. 3. Steps of specimen preparation.

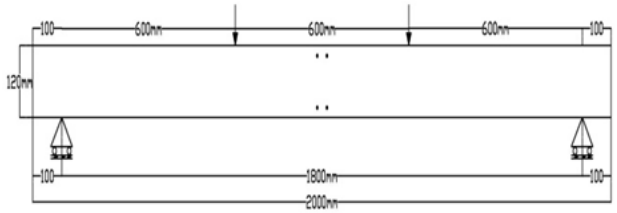

Fig. 4. Locations of demec points.

Fig. 5. Test setup.

4.1. Flexural serviceability load

The flexural serviceability load was calculated from the load-deflection curves. It is defined as the load corresponding to deflection equal to the span of the panel divided by (constant=250) according to The Egyptian Code. Fig. 6 represents the values for the serviceability load for all the tested panels. The main aim of calculating serviceability load is to evaluate the effect of using different meshes.

4.2. Ductility ratio

Ductility ratio is defined here as the ratio between the mid span deflection at ultimate load to that at the first crack load ($\Delta u/\Delta y$), panels reinforced with expanded metal mesh and welded steel meshes were given higher ductility ratio than control beam. Fig. 7 shows ductility ratios for all tested panels.

4.3. Energy absorption

Energy absorption is defined as the area under the load–deflection curve. Microsoft Office (excel sheet) was used to calculate the area under curve by integrated the equation of the load–deflection curve for each beam specimens as follow: ultimate load Energy absorbed = $\int_0^{\Delta u} f(\Delta)d\Delta$; where $f(\Delta)$ is the equation of load–deflection curve, and Δu is the mid-span deflection at failure load. Panels reinforced with expanded steel mesh were achieved higher energy absorption than control panels. Fig. 8 emphasizes energy absorption for all tested panels.

Table 4. Test results for all experimental test specimens.

Specimens designation	Code of panels	First crack load (kN)	Serviceability load (kN)	Ultimate load (kN)	First crack deflection (mm)	Maximum deflection (mm)	Ductility ratio	Energy absorption (kN.mm)
A	O1	12	29.00	36	2.55	16.08	6.30	433.70
	O2	12	28.10	34	2.11	14.71	6.97	375.79
B	E1	8	20.00	38	1.56	21.10	13.52	507.46
	E2	16	29.80	50	2.79	35.27	12.64	1317.19
C	W2	8	32.12	38	1.22	16.50	13.52	454.08
	W3	10	30.69	42	1.42	19.64	13.83	599.20
	W4	12	30.90	44	1	18.97	18.97	602.10
D	M1	8	24.30	40	1.28	23.64	18.46	667.88
E	T1	8	22.50	32	1	18.20	18.20	408.02
	T2	10	22.20	34	2.42	35.60	14.71	937.20

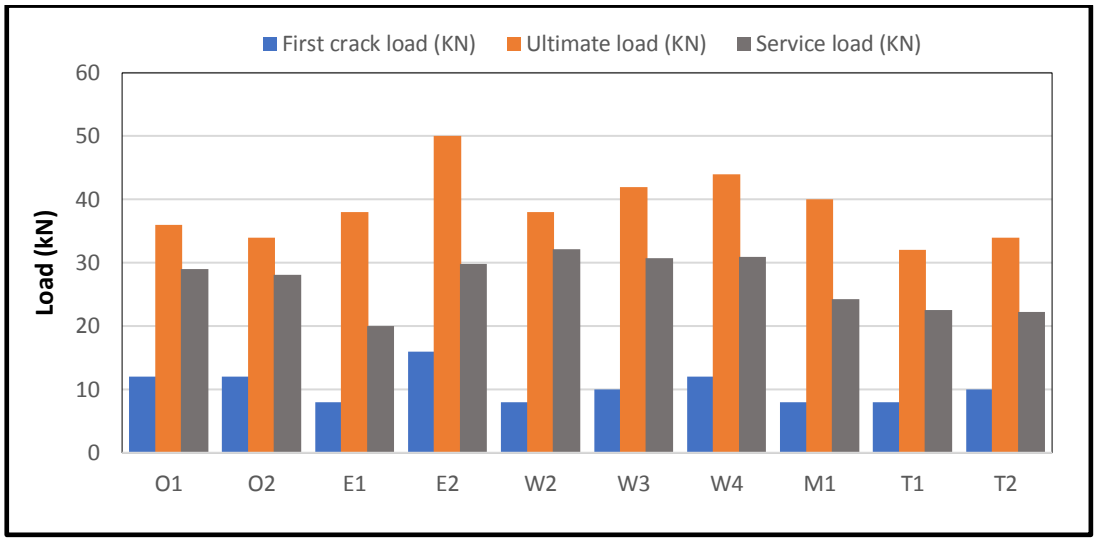

Fig. 6. First crack load, ultimate load and service load of all tested slabs.

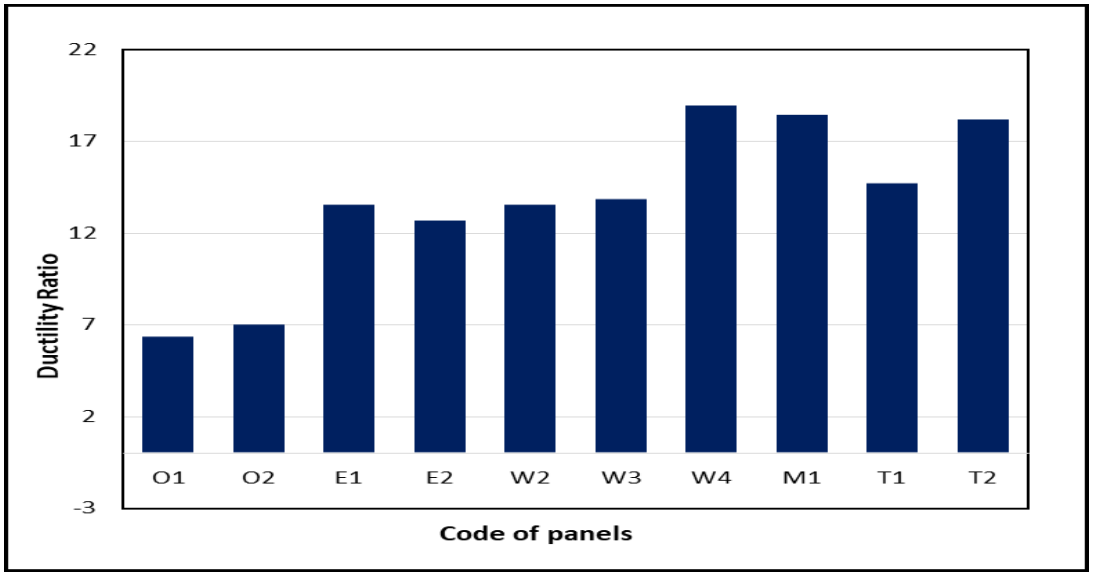

Fig. 7. Ductility ratio of all tested panels.

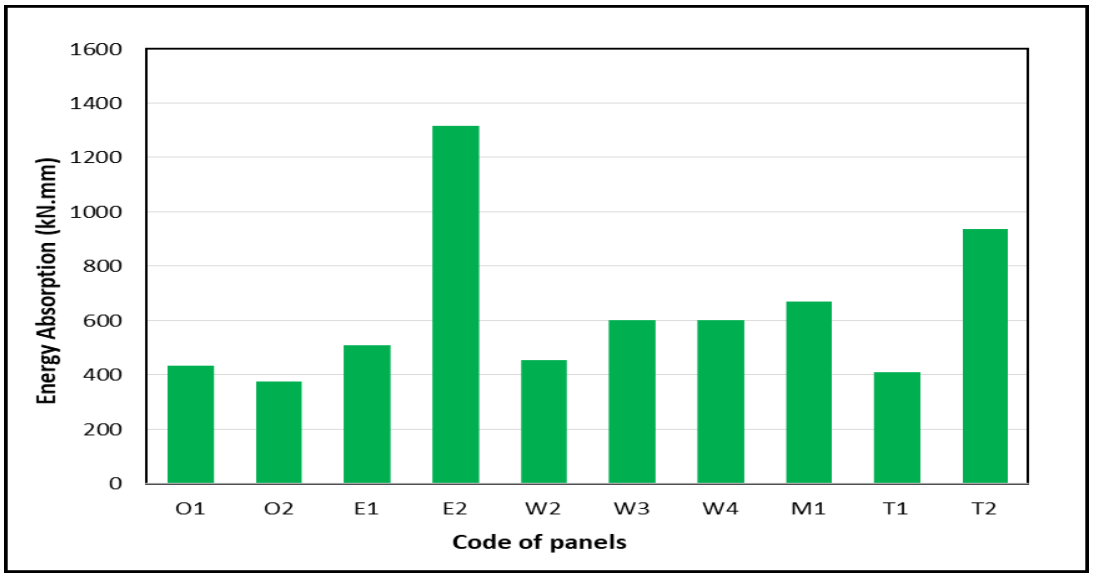

Fig. 8. Energy absorption for all tested panels.

4.4. Load-deflection relationship

Fig. 9 shows the load-deflection curves of the control specimen with fiber (O1) and control specimen without fiber (O2). From figure, group A, the ultimate load for specimen (O1) is more than that of the specimen (O2). This is due to the fiber used in the mix. The percentage of increasing in the ultimate load is 5.5%. Also the deflection of specimen (O2) is decrease by 8.51% compared to specimen (O1). From Fig. 10, group B, the specimens reinforced with expanded steel mesh in addition to steel bars (E1) and (E2). The ultimate load for specimen (E2) is more than that of specimen (E1). This is due to increasing the number of layers. The percentage of increasing in the ultimate load is 31.5%. Also the deflection of specimen (E1) is decrease by 40.1% compared to specimen (E2). Fig. 11 illustrates that, group C, the specimens reinforced with welded wire mesh in addition to steel bars (W2), (W3) and (W4). The ultimate load for specimen (W4, W3) is more than that of specimen (W2). This is due to increasing the number of layers. The percentage of increasing in the ultimate load is 15.7%, 10.5% respectively. Also the deflection of specimen (W4, W3) is increase by 14.9%, 19.09% respectively compared to specimen (W2). Fig. 12 illustrates that, group E, the specimens reinforced with Tenax mesh in addition to steel bars (T1) and (T2). The ultimate load for specimen (T2) is more than that of specimen (T1). This is due to increasing the number of layers. The percentage of increasing in the ultimate load is 6.25 %. Also the deflection of specimen (T2) is increase by 95.6% compared to specimen (T1). Fig. 13 emphasizes comparison of load deflection curves for all the tested panels.

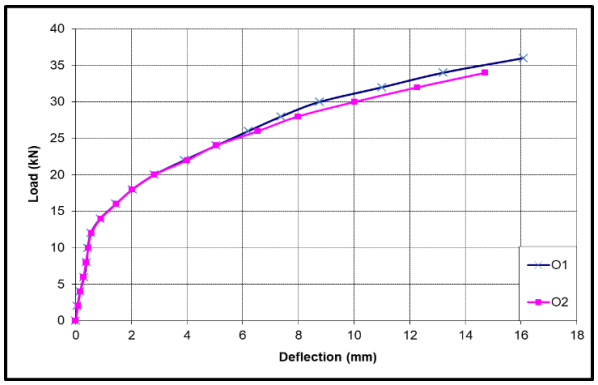

Fig. 9. Load-deflection curves for group (A).

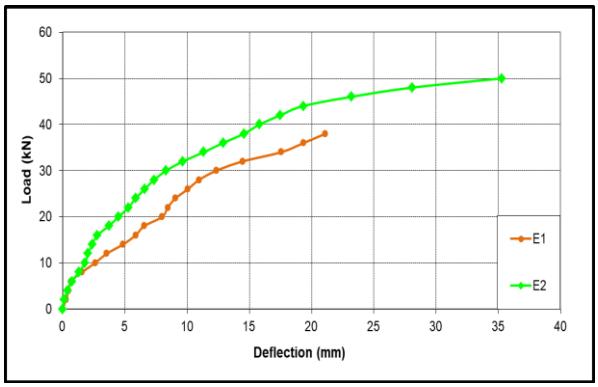

Fig. 10. Load-deflection curves for group (B).

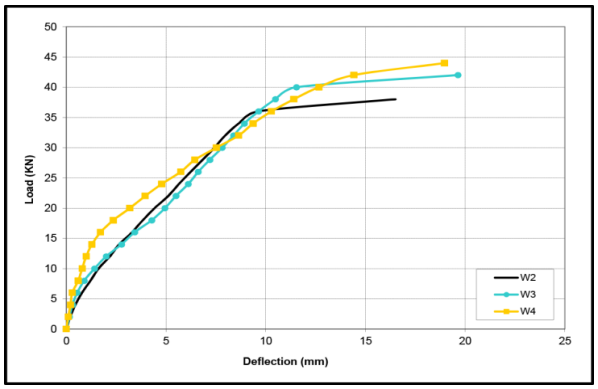

Fig. 11. Load-deflection curves for group (C).

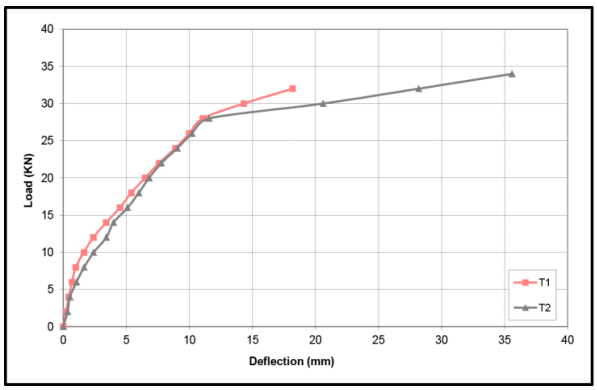

Fig. 12. Load-deflection curves for group (E).

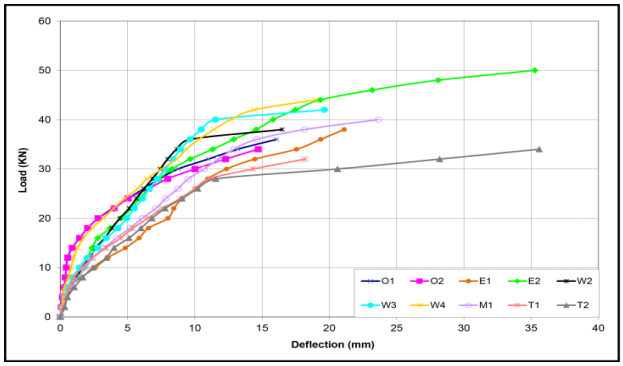

Fig. 13. Load-deflection curves for all tested panels.

4.5. Effect of using various types of meshes

In order to evaluate the effect of the reinforcing steel mesh type, specimens reinforced with expanded steel mesh, welded wire mesh and tenax mesh were compared to control specimen at the same number of layers. Fig. 14 illustrates the load-deflection curves of the control specimen with fiber (O1) is compared to the specimen reinforced with one layer of expanded steel mesh (E1) and the specimen reinforced with one layer of tenax mesh (T1). From figure, the ultimate load for specimen (E1) is more than that of (O1 and T1). This is due to the strength of expanded steel mesh. The percentage of increasing in the ultimate load is 5.5% and 18.7% respectively. Fig. 15 illustrates the load-deflection curves of the control specimen with fiber (O1) is compared to the specimen reinforced with two layers of expanded steel mesh (E2), two layers of welded wire mesh (W2), one layer of welded wire mesh plus one layer of expanded steel mesh (M1) and the specimen reinforced with two layers of tenax mesh (T2). From figure, the ultimate load for specimen (E2) is more than that of (O1, W2, M1 and T2). This is due to the strength of expanded steel mesh. The percentage of increasing in the ultimate load is 38.8%, 31.5% 25% and 47.05%, respectively.

In order to evaluate the effect numbers of steel wire mesh layers, specimens reinforced with expanded steel mesh, welded wire mesh and tenax mesh were compared to control specimen. Fig. 16 illustrates the load-deflection curves of the control specimen with fiber (O1) is compared to the specimen reinforced with one layer of expanded steel mesh (E1) and the specimen reinforced with two layers of expanded steel mesh (E2). From figure, the ultimate load for specimen (E2) is more than that of (O1 and E1). This is due to the number of layers. The percentage of increasing in the ultimate load is 38.8% and 31.5% respectively. Fig. 17 illustrates the load-deflection curves of the control specimen with fiber (O1) is compared to the specimen reinforced with two layers of welded wire mesh (W2), the specimen reinforced with three layers of welded wire mesh (W3) and the specimen reinforced with four layers of welded wire mesh (W4). From figure, the ultimate load for specimen (W4) is more than that of (O1, W2 and W3). This is due to the number of layers. The percentage of increasing in the ultimate load is 22.2%, 15.78% and 4.76%, respectively.

Fig. 18 illustrates the load-deflection curves of the control specimen with fiber (O1) is compared to the specimen reinforced with two layers of tenax mesh (T2), the specimen reinforced with one layer of tenax mesh (T1). From figure, the ultimate load for specimen (O1) is more than that of (T1, T2). The percentage of increasing in the ultimate load is 12.5% and 5.8% respectively.

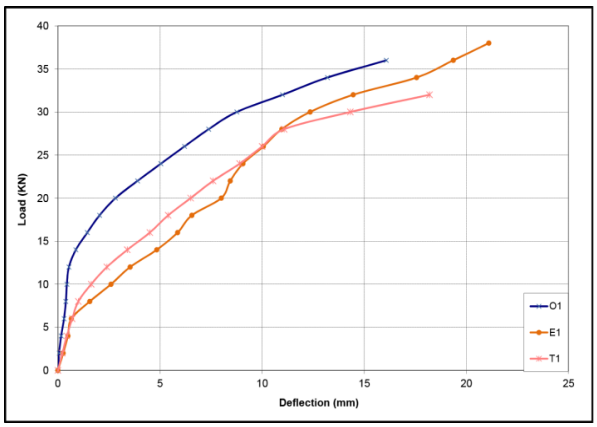

Fig. 14. Effect of type of reinforcement on the load–deflection for the panels.

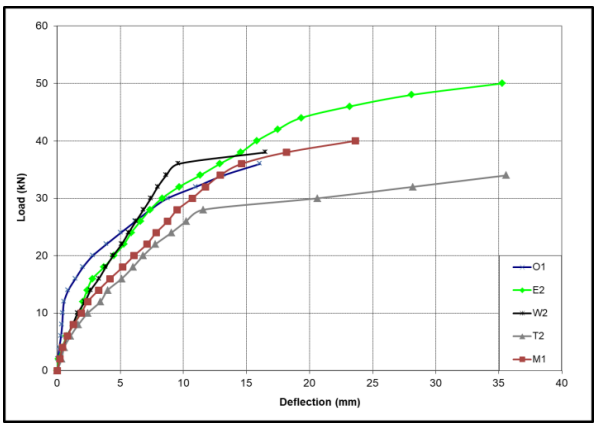

Fig. 15. Effect of type of reinforcement on the load-deflection for the panels.

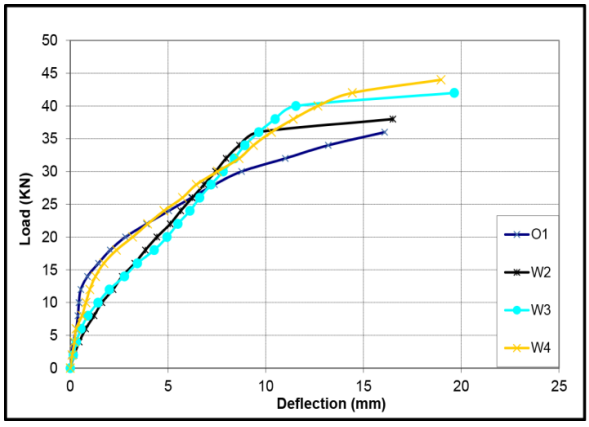

Fig. 16. Effect of number of layers of welded mesh for the panels.

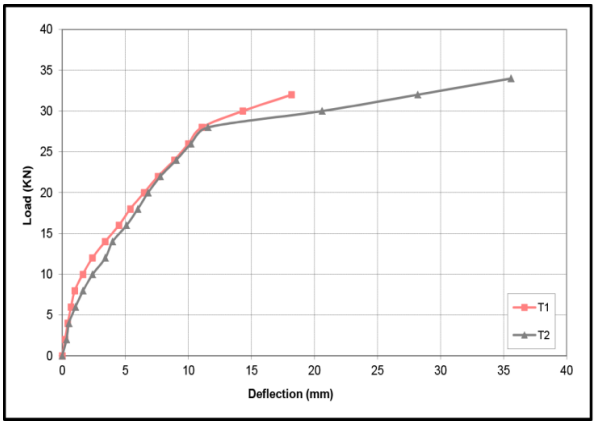

Fig. 17. Effect of number of layers of welded mesh for the panels.

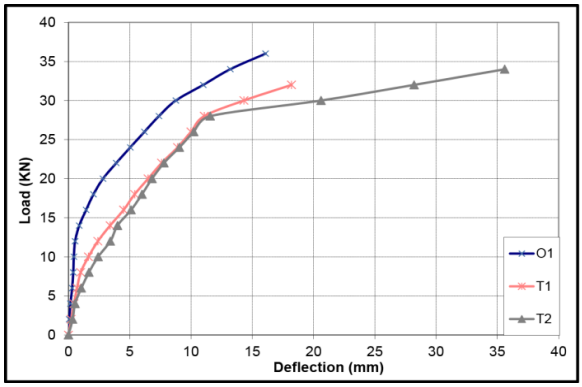

Fig. 18. Effect of number of layers of welded wire mesh for the panels.

4.6. Compressive and tensile strain

Fig. 19 shows load-strain curves for control group (A) specimens (O1 and O2). For panel O1, the compressive strain increased with the increase of the applied load. The maximum compressive strain reached about -0.00142 at maximum load 36 kN. However, the max tensile strain was 0.0015 at the same load. The maximum compressive strain at panel O2 reached about -0.0014at maximum load 34 kN. However, the max tensile strain was 0.00136 at the same load.

The load-compressive and tensile strain curves for group B (panels E1, E2) are plotted in Fig. 20. The curves show that the compressive strain increased with the increase of the applied load. At panel E1 the maximum compressive strain reached about -0.0025 at maximum load 38 kN. However, the max tensile strain was 0.0023 at the same load. For panel (E2), the maximum compressive strain reached about -0.0031 at maximum load 50 kN. However, the max tensile strain was 0.003 at the same load.

For group C (panels W2, W3 and W4), the compressive strain increased with the increase of the applied load. For panel (W2), the maximum compressive strain reached about -0.0015 at maximum load 38 kN. However, the max tensile strain was 0.002 at the same load. The maximum compressive strain at panel W3 reached about -0.00142 at maximum load 42 kN. However, the max tensile strain was 0.00135 at the same load. The maximum compressive strain at panel W4 reached about -0.00255 at maximum load 44 kN. However, the max tensile strain was 0.0025 at the same load as shown in Fig. 21.

For the last group specimens E (specimens T1 and T2), Fig. 22 shows that the compressive strain increased with the increase of the applied load. For panel (T1) the maximum compressive strain reached about -0.0017 at maximum load 32 kN. However, the max tensile strain was 0.00168 at the same load. The maximum compressive strain at panel (T2) reached about -0.0022 at maximum load 34 kN. However, the maximum tensile strain was 0.00217 at the same load.

4.7. Cracking patterns and mode of failure

Cracks were traced and marked throughout the side of the specimen. The first crack-load of each specimen, crack propagation, and failure mode were recorded. Flexural cracks developed near the mid-span of the specimen. With the increase of the load, the cracks propagated vertically and new flexural cracks were developed rapidly. The cracks started to propagate wider when the specimens approached their failure load. As the load increased, more cracks started to develop and the crack at midspan started to propagate vertically towards the top surface of the specimen, while most of the developed cracks did not continue propagating. This could be attributed to the effect of steel mesh in controlling the crack width. The cracks for all tested panels can be shown in Fig. 23.

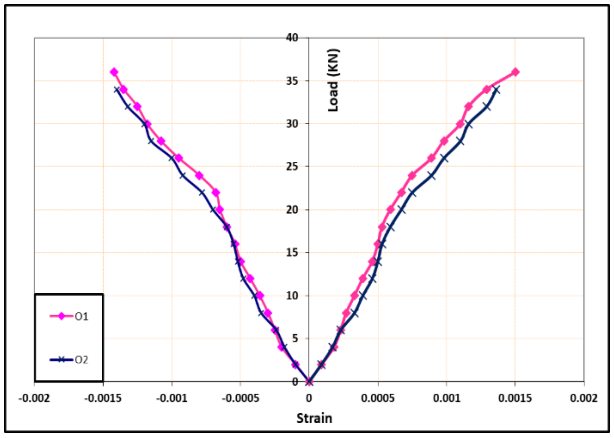

Fig. 19. Load-compressive and tensile strain curves for group (A).

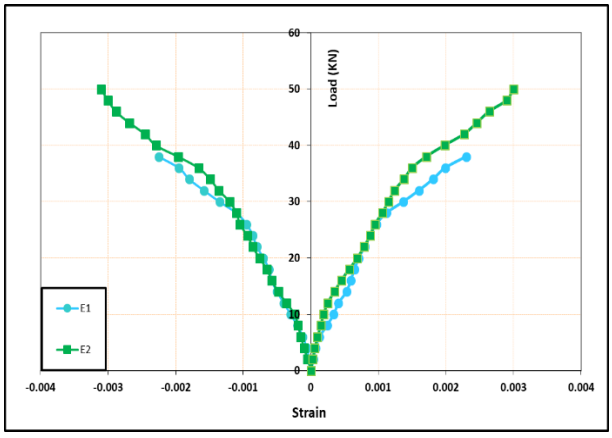

Fig. 20. Load-compressive and tensile strain curves for group (B).

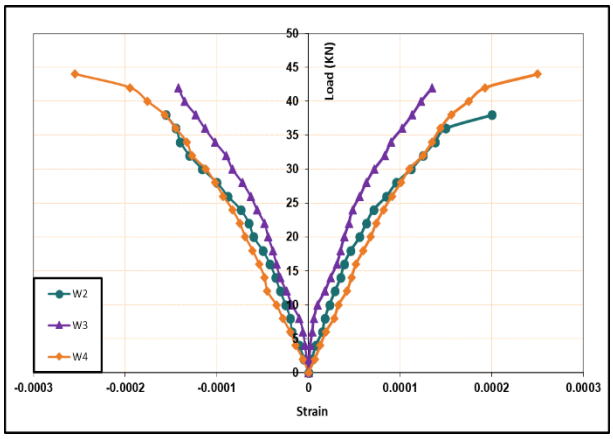

Fig. 21. Load-compressive and tensile strain curves for group (C).

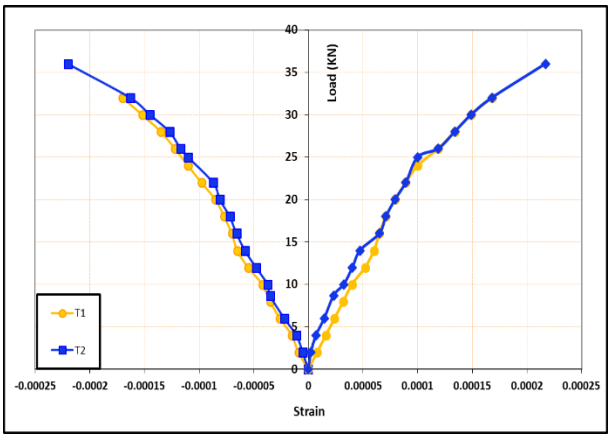

Fig. 22. Load-compressive and tensile strain curves for group (E).

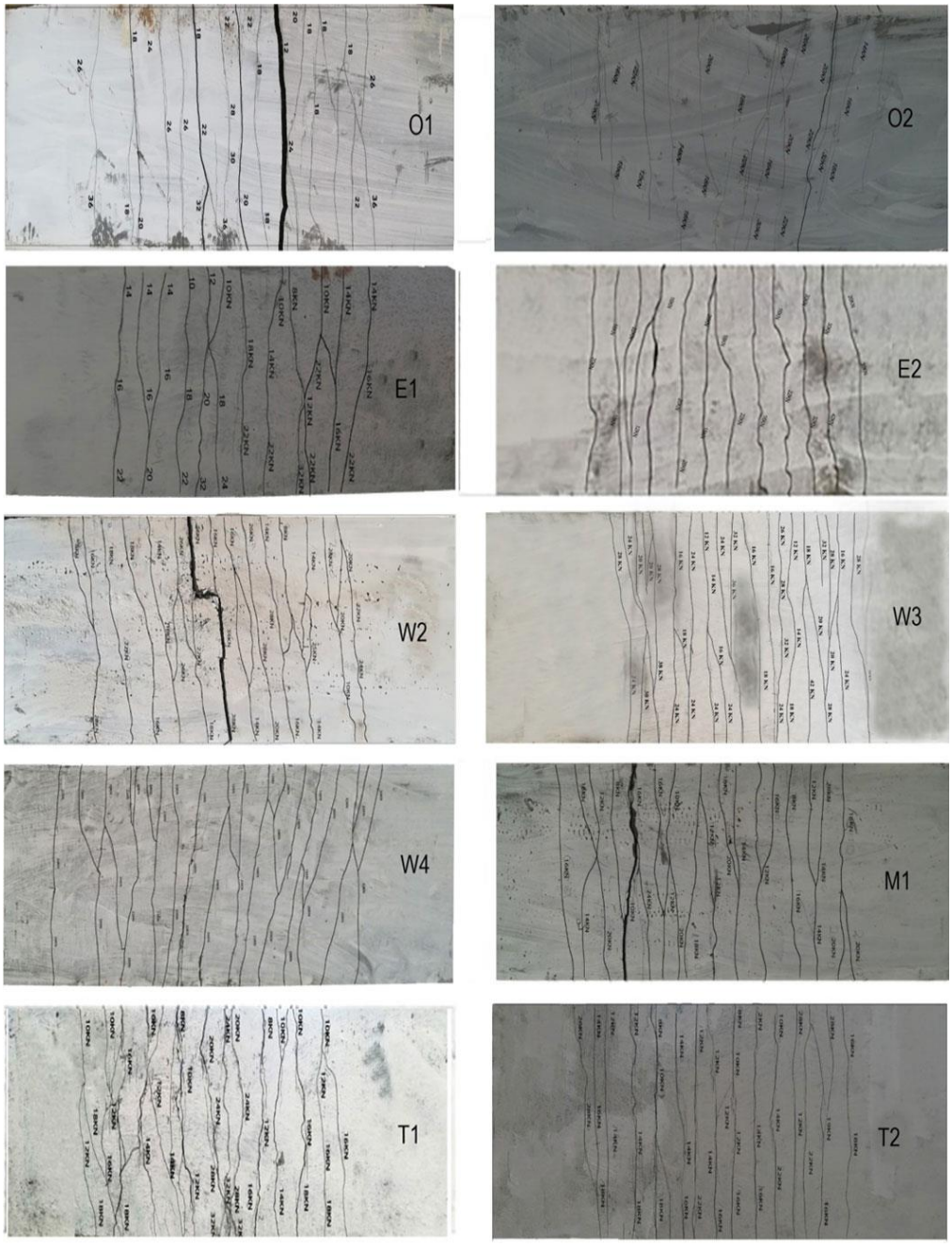

Fig. 23. Cracking patterns for all tested panels.

5. Finite Element Simulation

The specimens of study were modeled as 3D structures in Abaqus. Concrete parts were modeled using C3D8R. Steel bars, welded, expanded steel mesh and tenax mesh were modeled using T3D2 elements. (Fig. 24) shows modeling of all parts (reinforced concrete hollow-core panels, Steel bars, welded, expanded metal mesh, tenax mesh) in Abaqus.

The supports of the concrete panels were prevented from transferring to YZ directions and from rotation about XZ direction at the two lines of contact with underneath roller supports. Concrete panel is exposed to two concentrated loads at equivalent distance from the support line.

Concerning the interaction between the loads, reinforced mesh and concrete target general, contact surfaces of the concrete target can be defined using the Interaction, Create Interaction Property and Create Interaction option. We specify all regions of the model that can potentially come into contact with each other by defining contact surfaces.

6. FE Model Verification

Fig. 25 represents a comparison between failure modes and cracks pattern of the tested beam as published and the corresponding FE models.

The load-deflection curve of experimental work and its associated FE model are shown in Fig. 26.

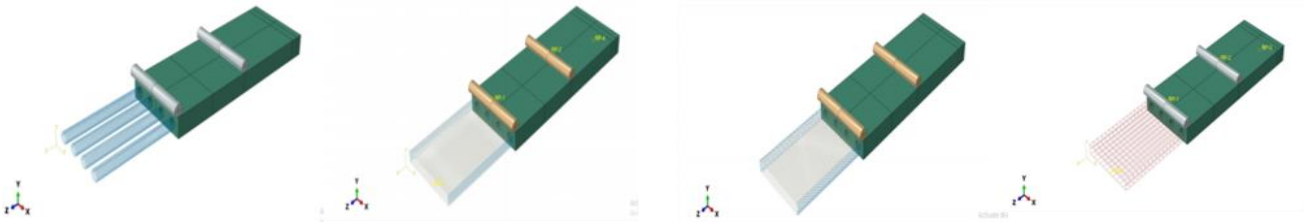

circular mesh welded metal mesh expanded metal mesh tenax mesh

Fig. 24. Modeling of reinforcing metal mesh.

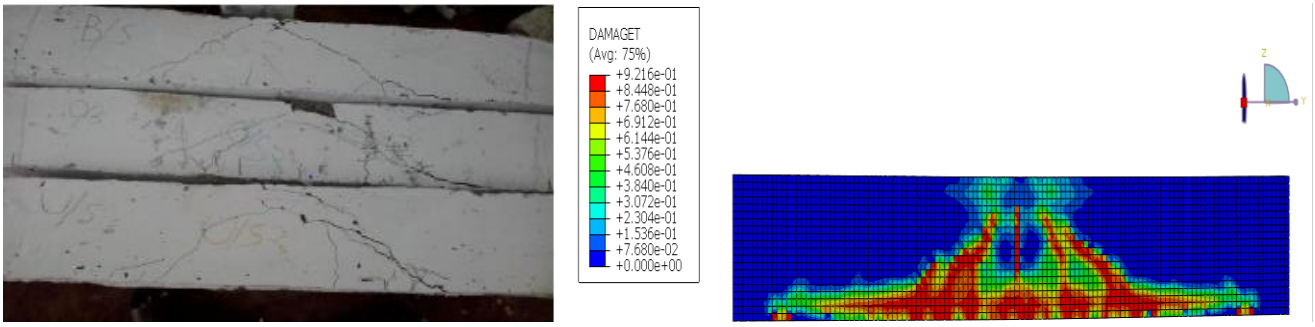

a) Failure shape of experimental model b) Failure shape of FE model

Fig. 25. Failure pattern of model.

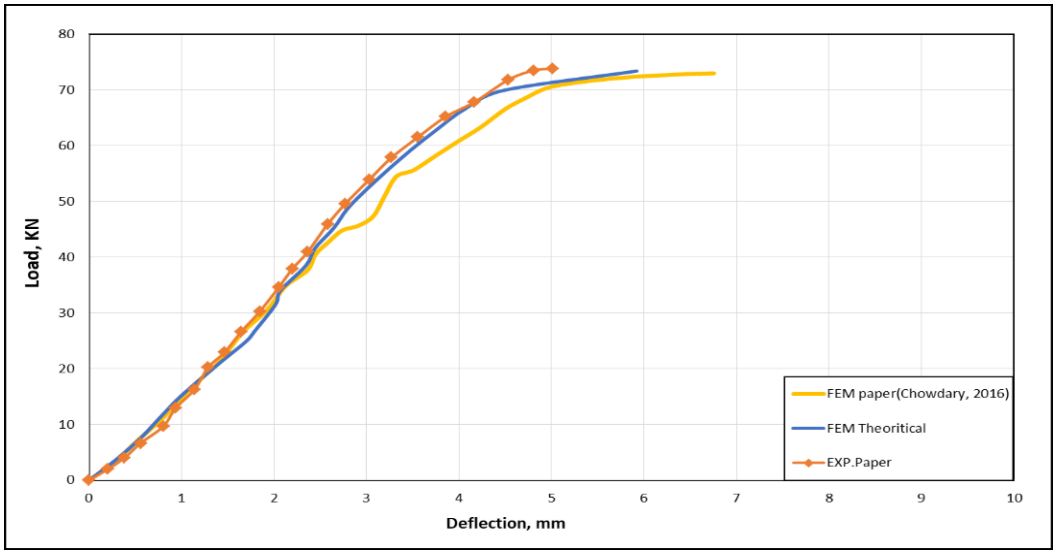

Fig. 26. Load-deflection curve of experimental work and their corresponding FE model.

7. Comparison between Experimental and FE Simulation Results

The comparison between experimental and FE simulation results, ultimate load, 1st crack load, mid span deflection at the ultimate load are illustrated in Table 5. Fig. 27 and Fig. 28 presents the applied load-mid span deflection, and the applied load-strain curves; respectively as obtained from the experimental and theoretical results for the all tested panels. The first crack load was determined as the first deviation from linearity of load deflection curve. The comparison between the experimental and theoretical cracking patterns for all tested specimens are presented in Fig. 29. Stress distribution for all tested panels can be obtained at Fig. 30.

Consequently, it can be concluded that the FE simulations give accurate results in comparing with the experimental results. In addition, these comparisons indicate a good agreement in slope of curves in the linear stage. For nonlinear stage, and due to the possibility of the inaccuracy in modelling the post yield behaviour of steel rebar material, there is somewhat none agreement between the finite element results and those of experimental results.

Table 5. Comparison between experimental and theoretical results.

Specimens designation	Code of panels	First crack load (kN)			Ultimate load (kN)			Maximum deflection (mm)		
		Finite Element Method Results	Experimental Study Results	Percentage of difference	Finite Element Method Results	Experimental Study Results	Percentage of difference	Finite Element Method Results	Experimental Study Results	Percentage of difference
A	O1	12.75	12	1.062	35.85	36	0.995	15.44	16.08	0.960
	O2	12.29	12	1.024	34.85	34	1.025	14.26	14.71	0.969
B	E1	8.78	8	1.097	39.99	38	1.052	23.12	21.10	1.095
	E2	16.68	16	1.042	50.26	50	1.005	33.08	35.27	0.93
C	W2	8.72	8	1.09	39.29	38	1.033	16.52	16.50	1.001
	W3	10.85	10	1.085	43.35	42	1.032	18.76	19.64	0.955
	W4	12.94	12	1.078	44.5	44	1.011	17.91	18.97	0.944
D	M1	8.46	8	1.057	40.98	40	1.024	23.14	23.64	0.978
E	T1	8.83	8	1.103	32.92	32	1.028	17.30	18.20	0.950
	T2	10.8	10	1.080	34.15	34	1.004	34.10	35.60	0.957

8. Conclusions

Based on the results and observations of the theoretical and experimetal study presented in chapter the following conclusions could be drawn as follows:

- The best behavior of ferrocement hollow-cored panels was that of reinforced with two layers of expanded metal mesh in terms of ultimate load and Energy absorption.
- The specimen reinforced with two layers of expanded steel mesh increase the ultimate load by (31.5%) compared to that reinforced with one layer of expanded steel mesh. In addition, the specimen reinforced with four layers of welded wire mesh increase the ultimate load by (15.7% and 4.7%) compared to that reinforced with two layers of welded wire mesh and three layers of welded wire mesh, respectively.
- Using two layers of expanded steel mesh increased the ultimate load by percentage (38.8%) compared to control panel, while using two, three and four layers of welded wire mesh increased the ultimate load by percentage (5.5%, 16.6% and 22.2%) compared to control panel.
- The highest energy absorption property was shared between specimens made of two layers of expanded steel mesh and two layers of tenax mesh by percentage (67.07%, 53.7%) compared to control panel, respectively. and the lowest was found mostly with hollow-cored panels made of one layer of tenax by percentage (6.29%) compared to control panel.
- The highest Ductility ratio was shared between specimens made of four layers of welded wire mesh and specimen reinforced with one layer of expanded steel mesh + one layer of welded wire mesh by percentage (66.7%, 65.8%) compared to control panel, respectively.
- There is a great saving of weight by making voids area in the cross section leading to easy construction especially for weak soil foundations.
- Good agreement was founded between the theoretical and experimental results.
- Out of the point of this research, using ferrocement hollow-cored panels with different types and reinforced with several layers of mesh reinforcement may be have true construction merits for using in a variety of applications.

Further research needs to be conducted to reach sound recommendations for practical use especially for the beams with light polystyrene foam of high densities.

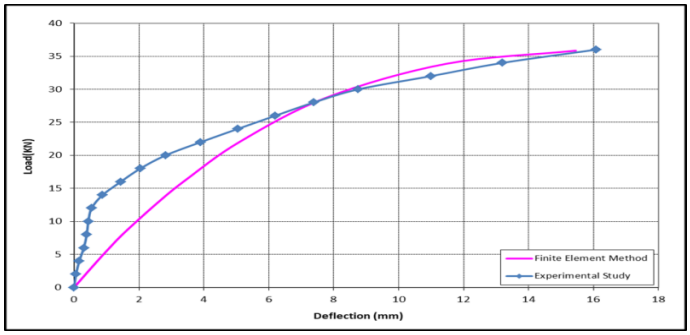

a) Load-deflection curves for panel O1

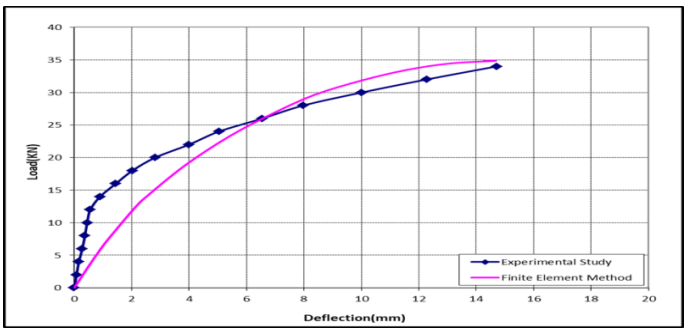

b) Load-deflection curves for panel O2

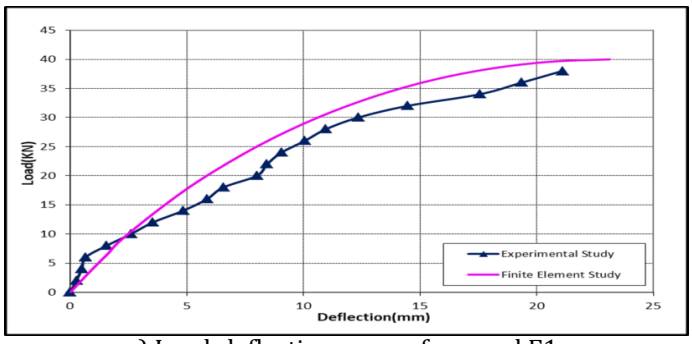

c) Load-deflection curves for panel E1

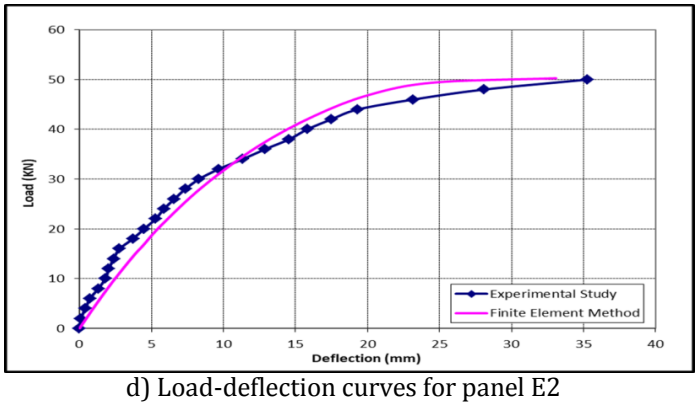

d) Load-deflection curves for panel E2

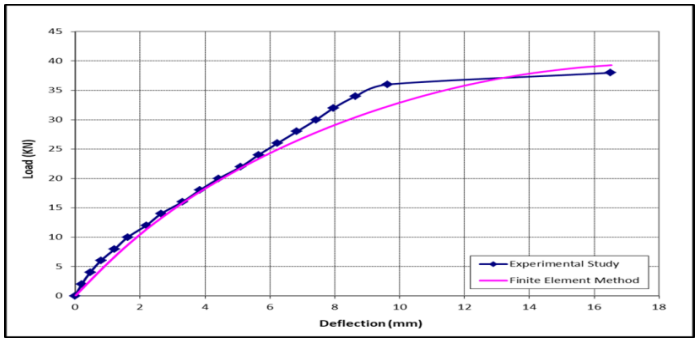

e) Load-deflection curves for panel W2

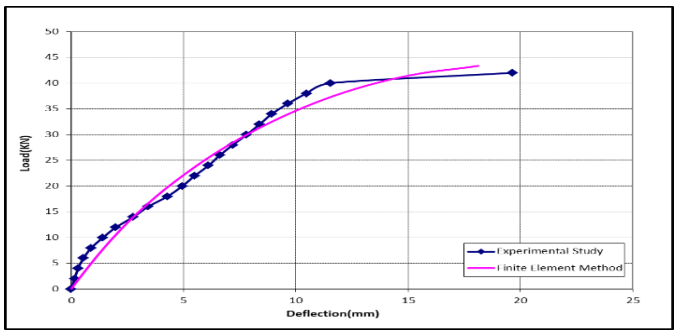

f) Load-deflection curves for panel W3

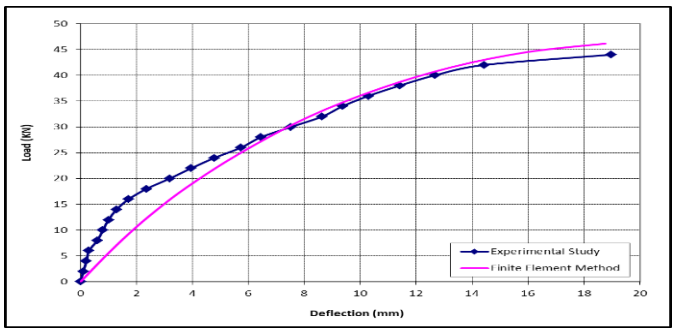

g) Load-deflection curves for panel W4

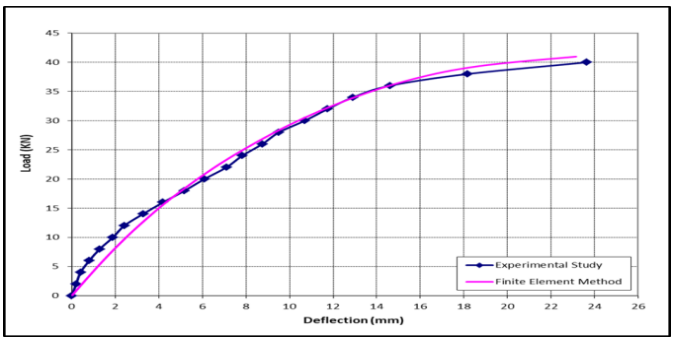

h) Load-deflection curves for panel M1

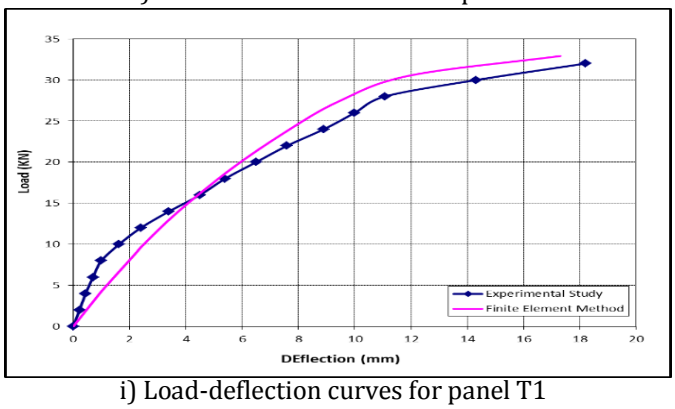

i) Load-deflection curves for panel T1

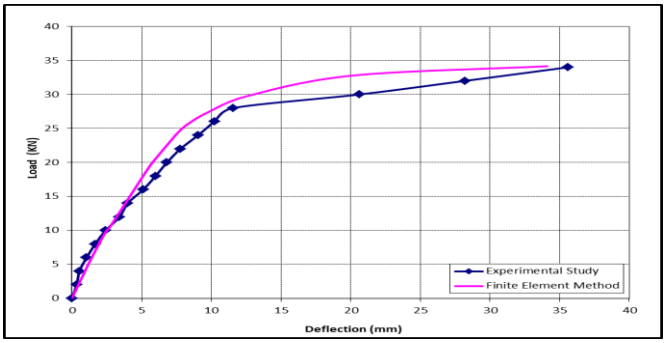

j) Load-deflection curves for panel T2

Fig. 27. Load-deflection curve for test specimens for experimental and theoretical results.

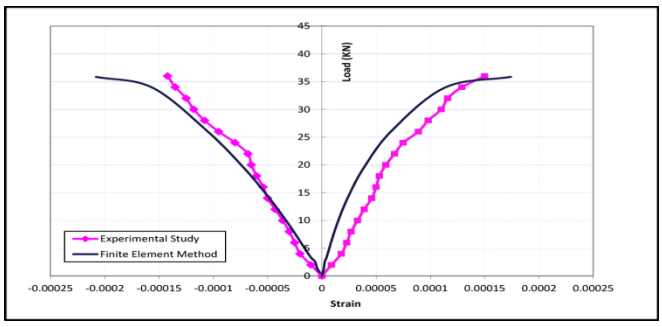

a) Load-strain curves of panel O1

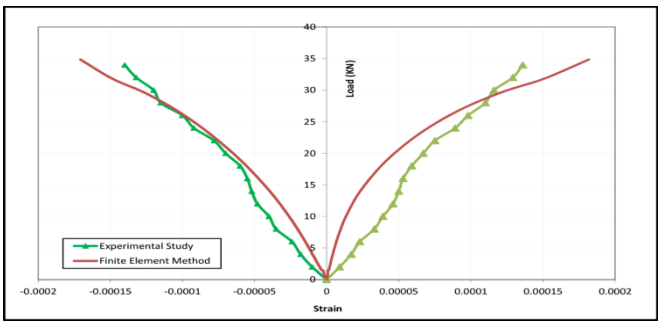

b) Load-strain curves of panel O2

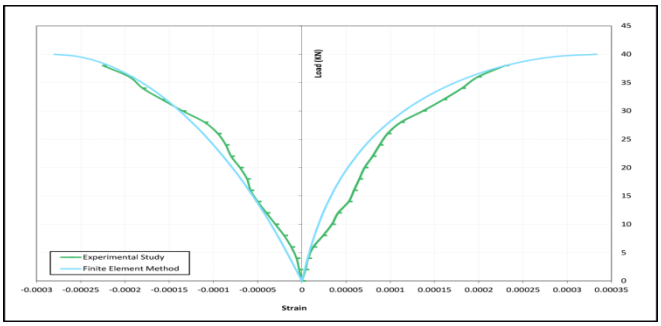

c) Load-strain curves of panel E1

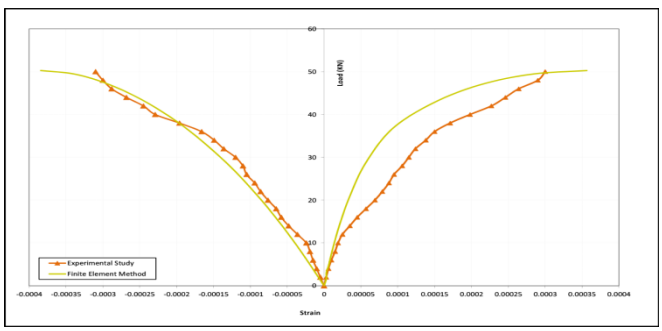

d) Load-strain curves of panel E2

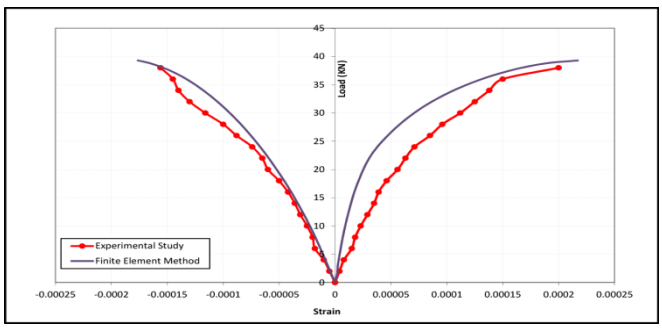

e) Load-strain curves of panel W2

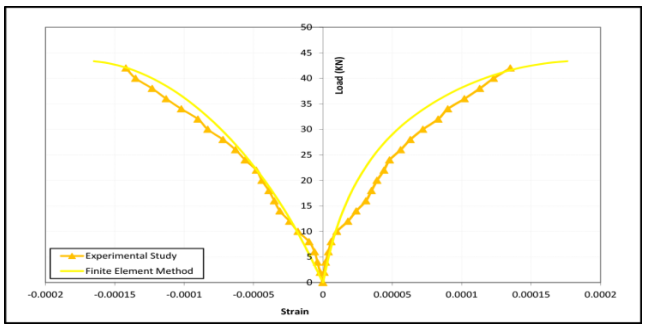

f) Load-strain curves of panel W3

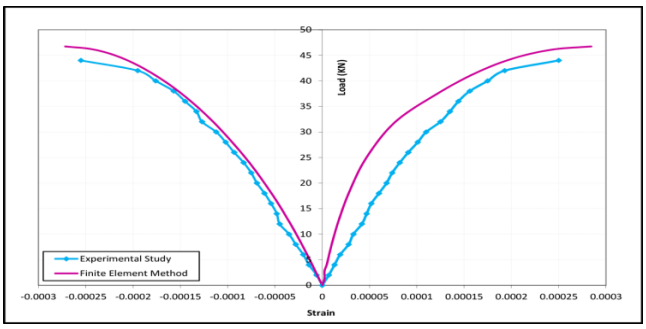

g) Load-strain curves of panel W4

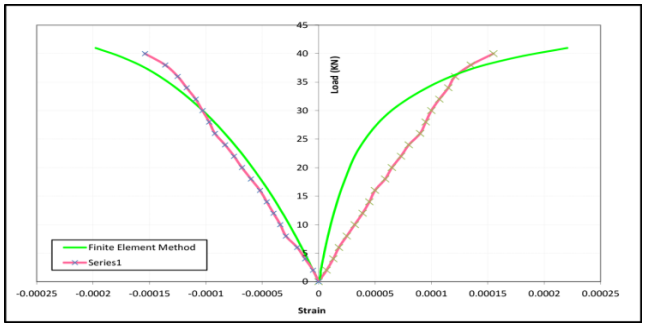

h) Load-strain curves of panel M1

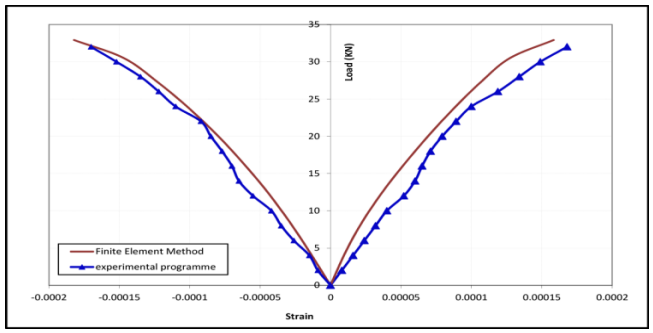

i) Load-strain curves of panel T1

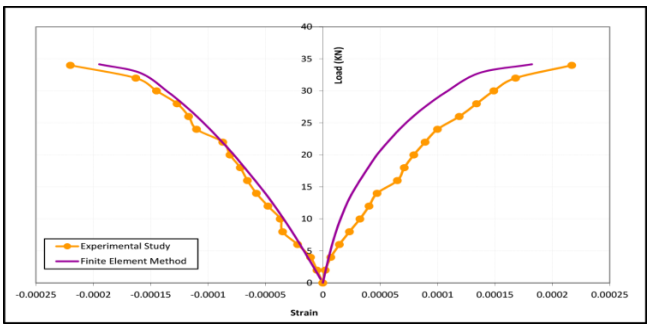

j) Load-strain curves of panel T2

Fig. 28. Load- strain curves for tested specimens and experimental and theoretical results.

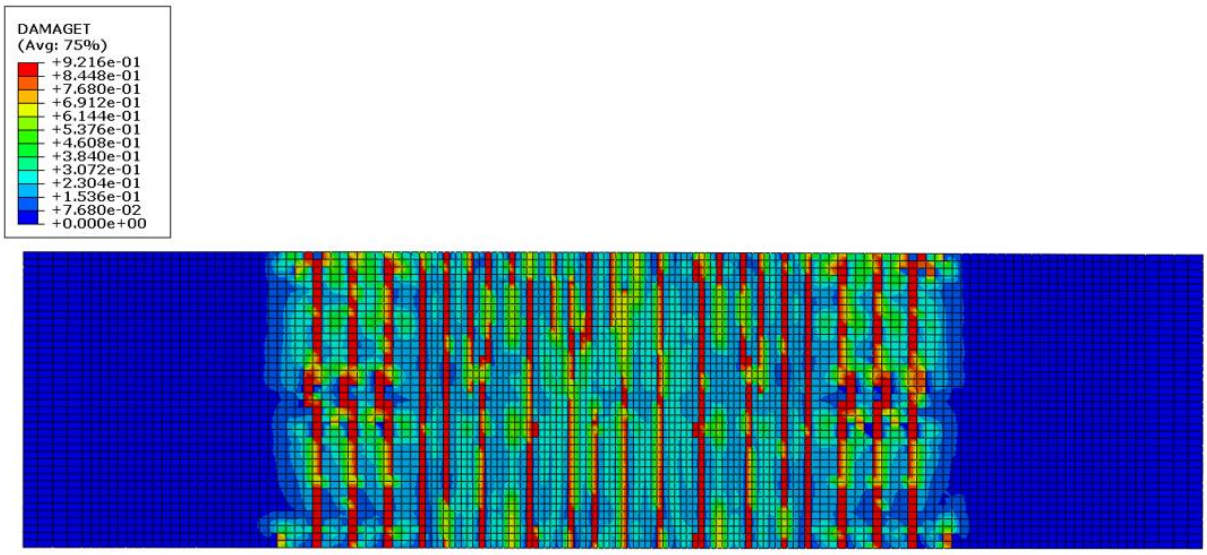

a) Cracking pattern for panel O1 from the theoretical study

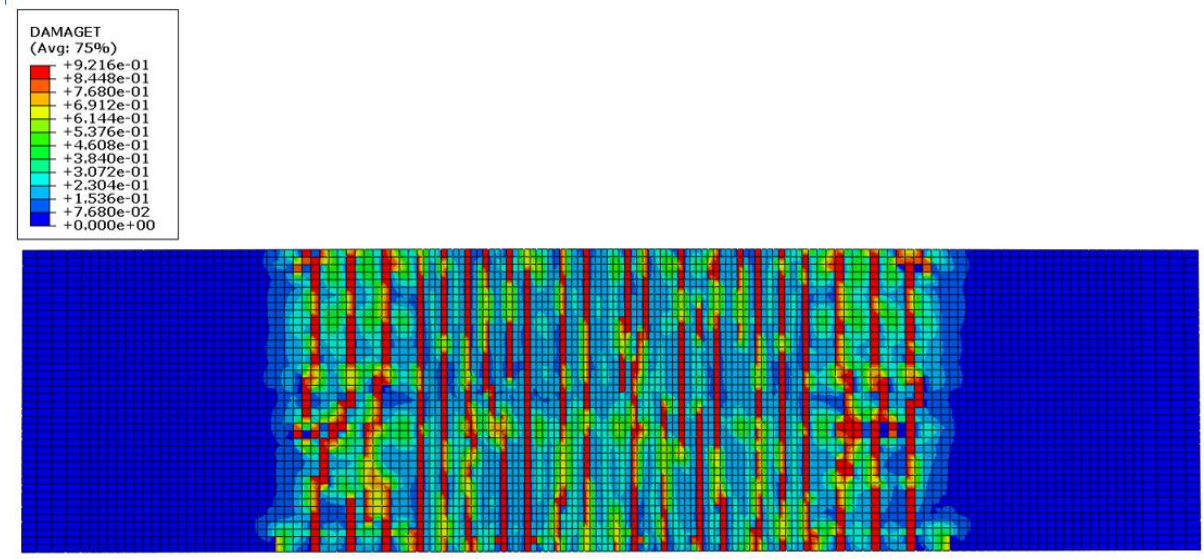

b) Cracking pattern for panel O2 from the theoretical study

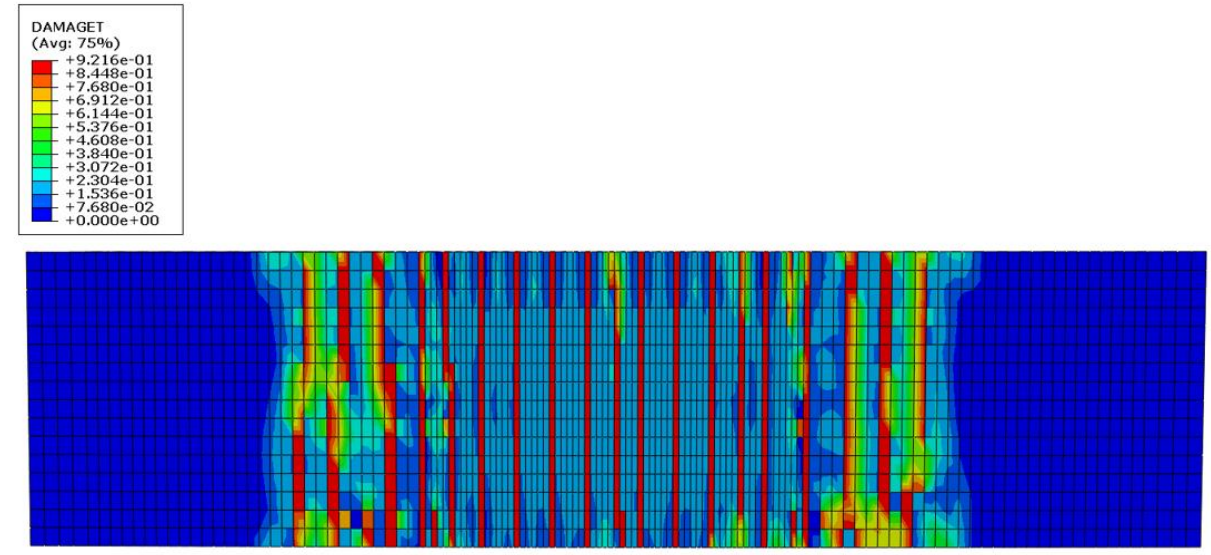

c) Cracking pattern for panel E1 from the theoretical study

Fig. 29. (continued)

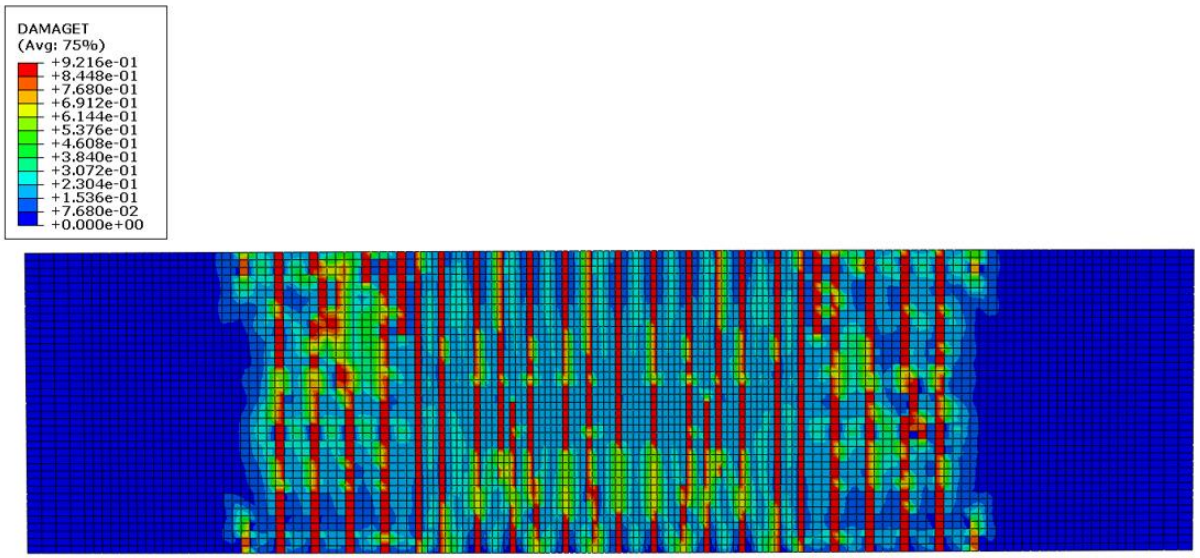

d) Cracking pattern for panel E2 from the theoretical study

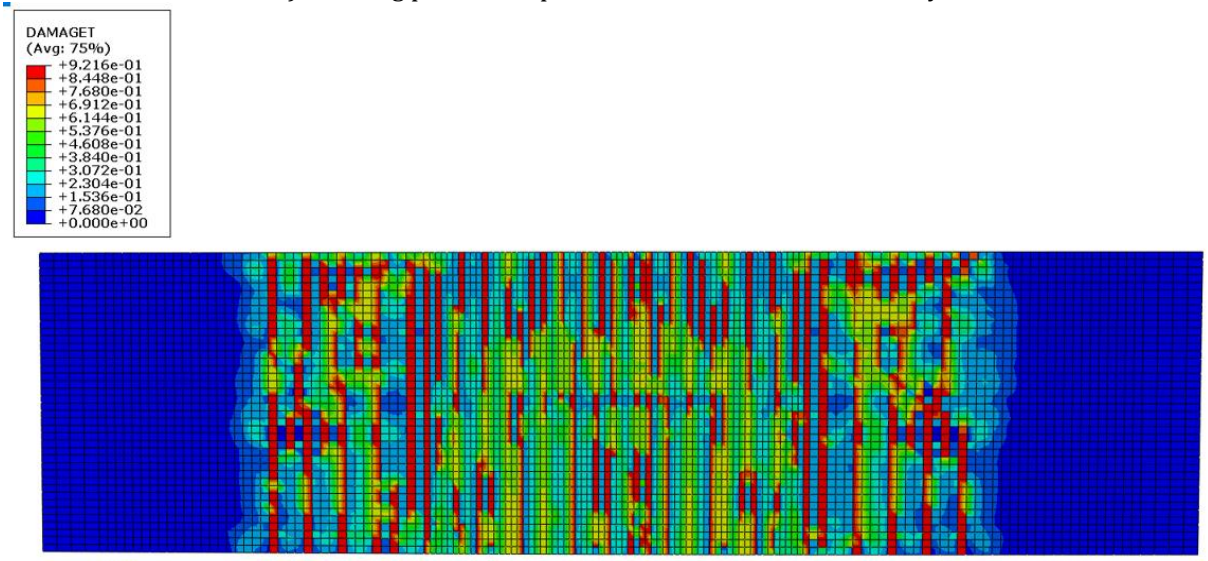

e) Cracking pattern for panel W2 from the theoretical study

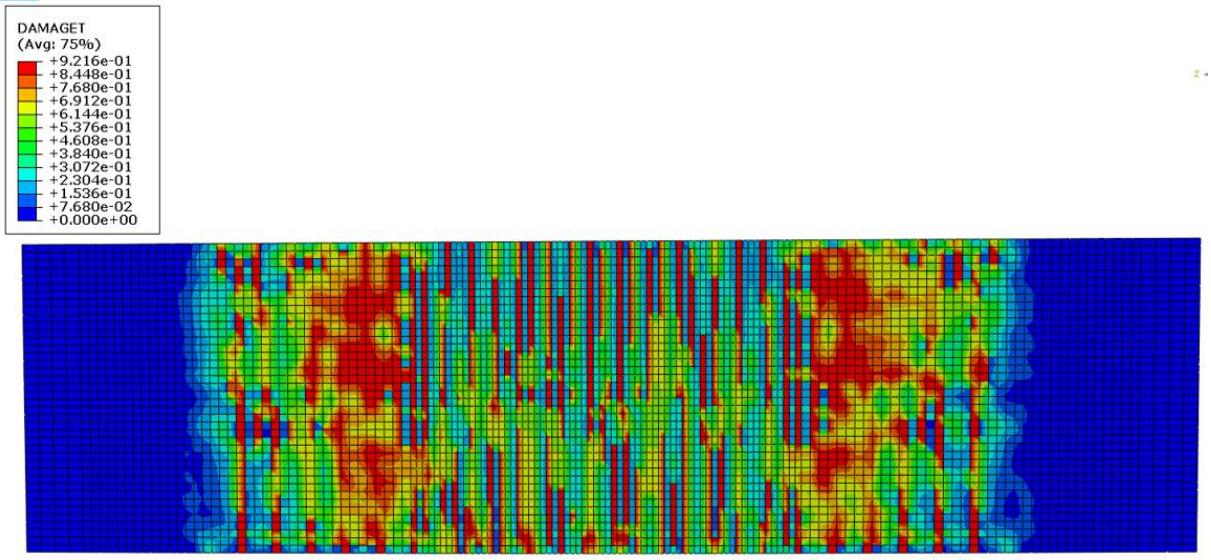

f) Cracking pattern for panel W3 from the theoretical study

Fig. 29. (continued)

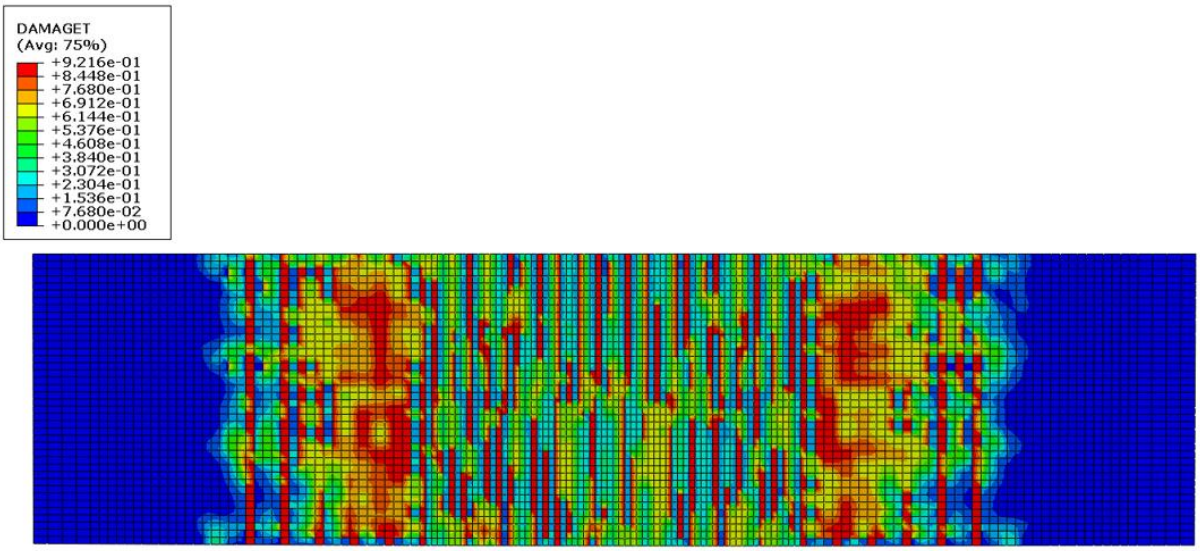

g) Cracking pattern for panel W4 from the theoretical study

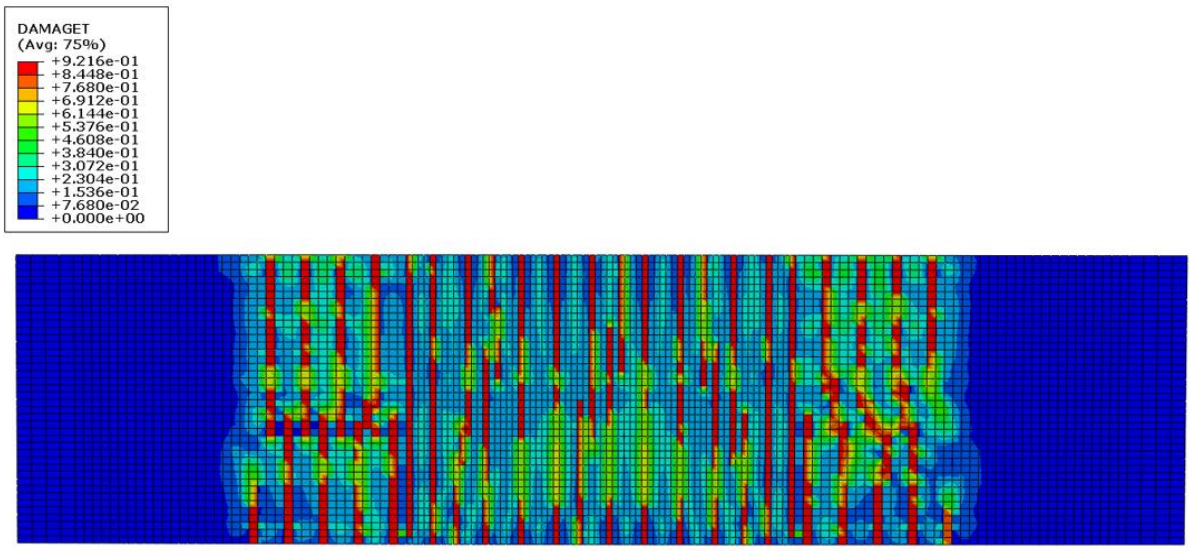

h) Cracking pattern for panel M1 from the theoretical study

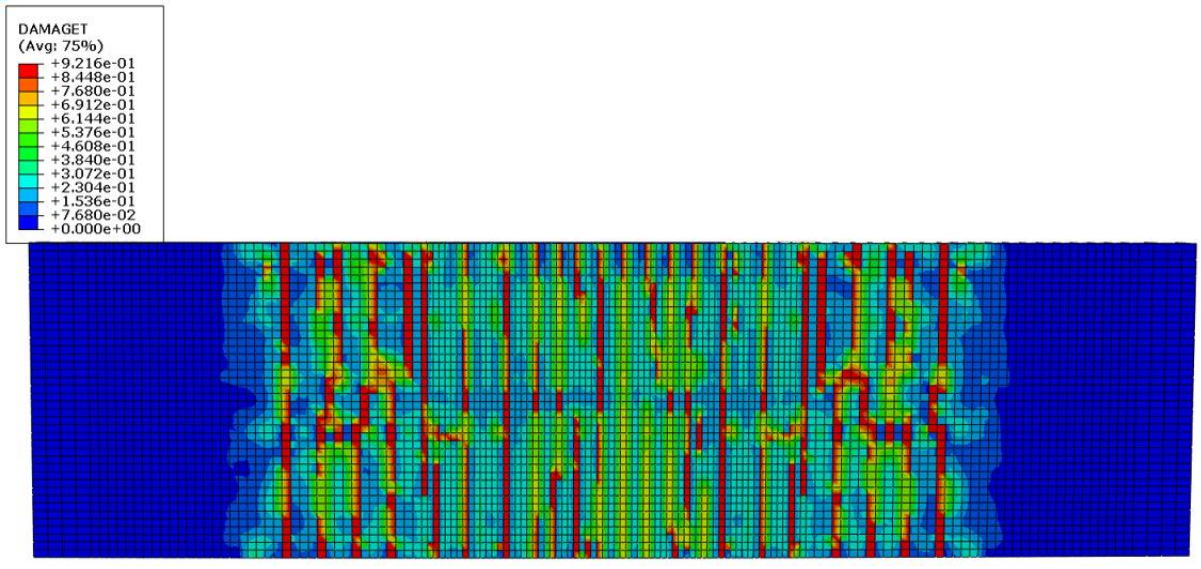

i) Cracking pattern for panel T1 from the theoretical study

Fig. 29. (continued)

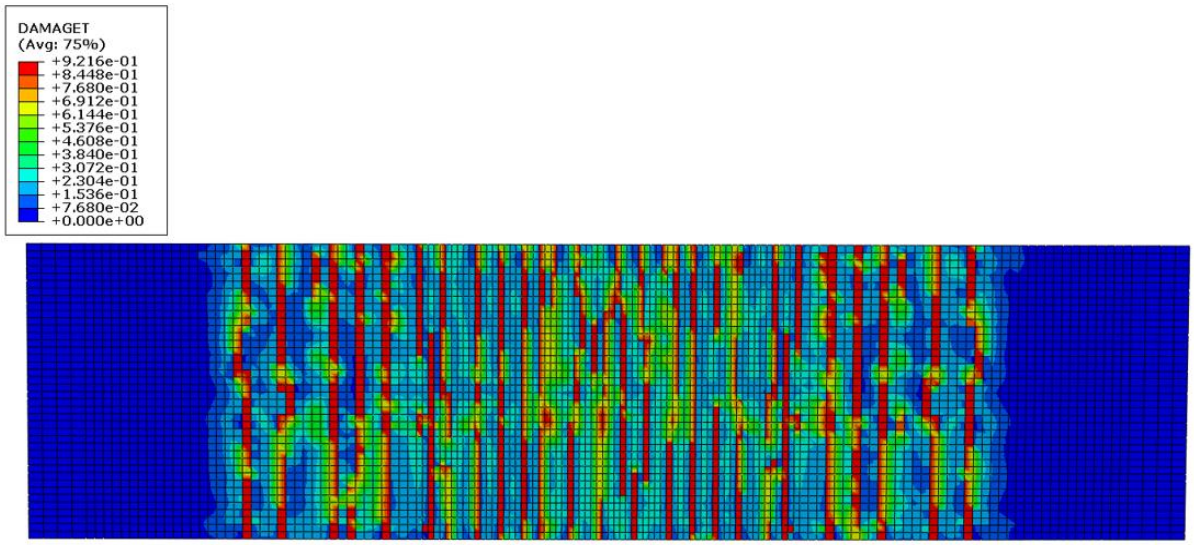

j) Cracking pattern for panel T2 from the theoretical study

Fig. 29. Cracking patterns for all tested specimens from the theoretical study.

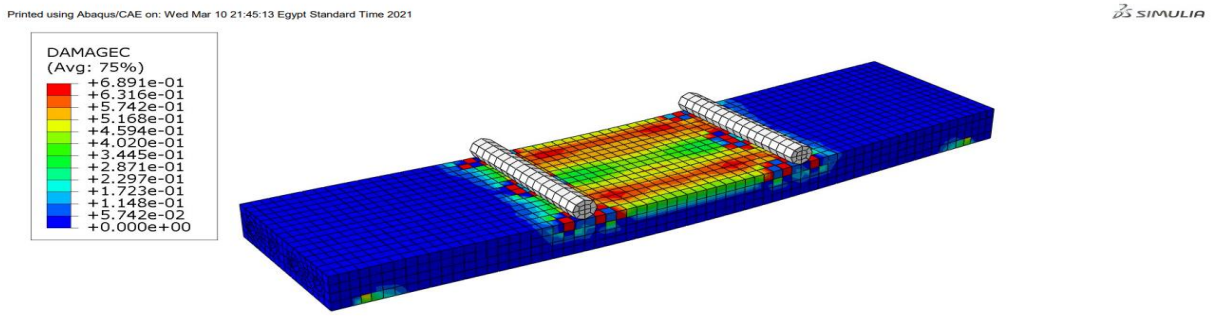

a) Stress distribution for panel O1 from the theoretical study

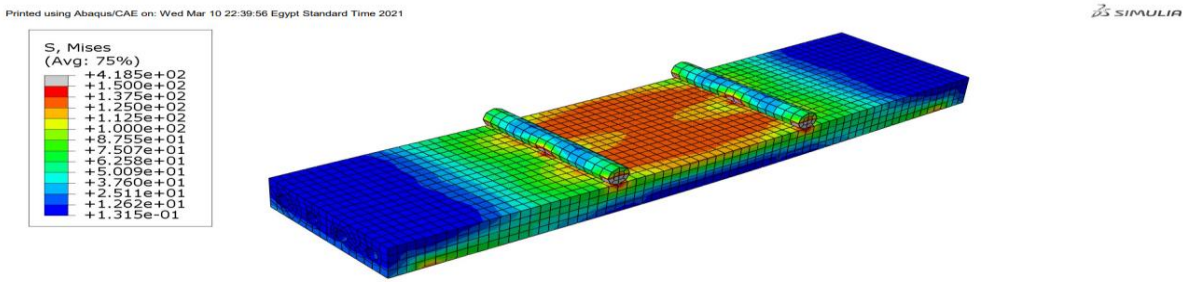

b) Stress distribution for panel O2 from the theoretical study

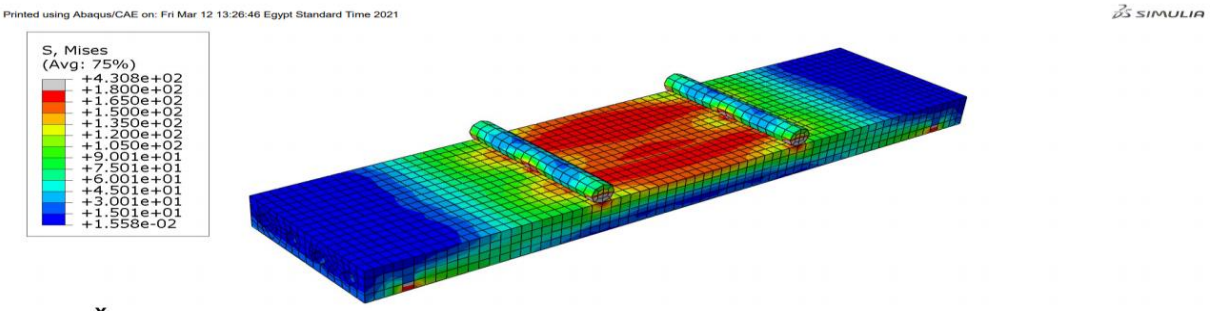

c) Stress distribution for panel E1 from the theoretical study

Fig. 30. (continued)

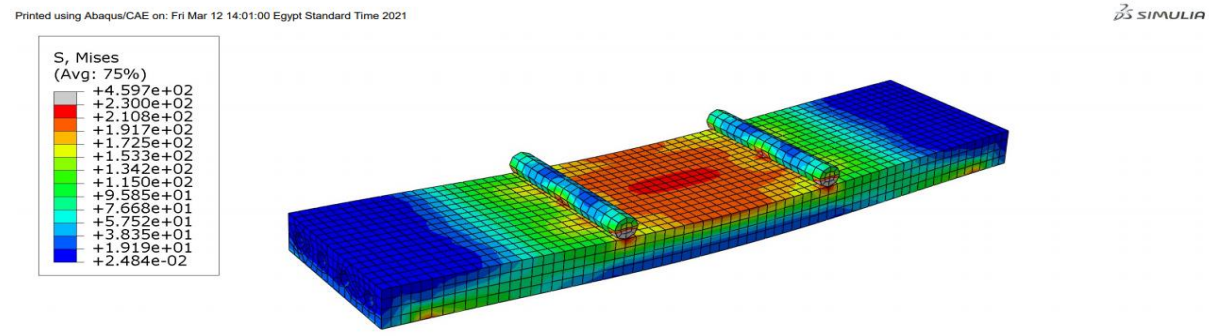

d) Stress distribution for panel E2 from the theoretical study

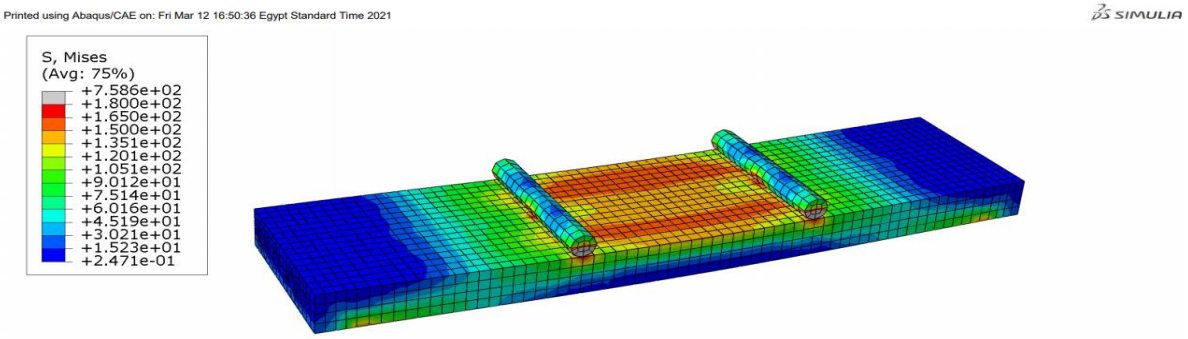

e) Stress distribution for panel W2 from the theoretical study

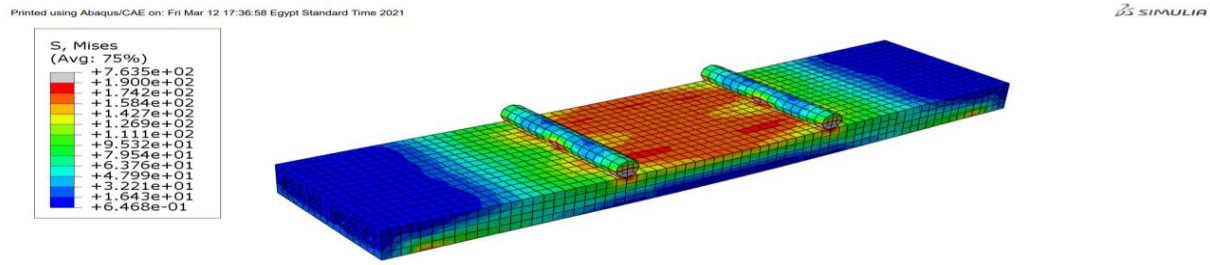

f) Stress distribution for panel W3 from the theoretical study

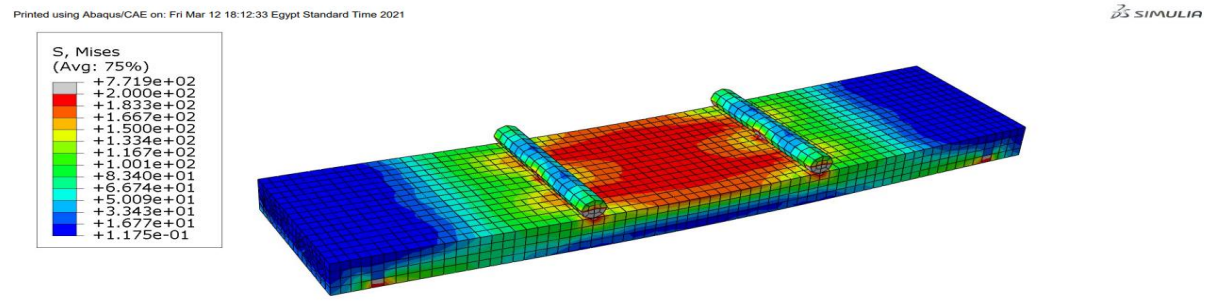

g) Stress distribution for panel W4 from the theoretical study

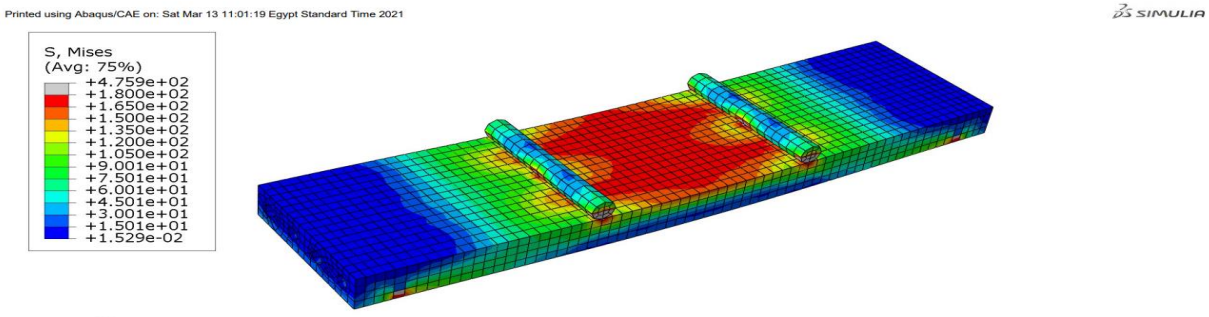

h) Stress distribution for panel M1 from the theoretical study

Fig. 30. (continued)

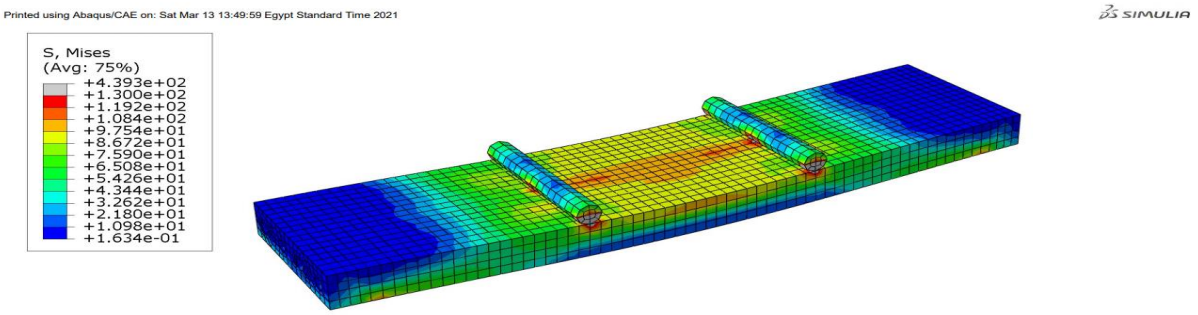

k) Stress distribution for panel T1 from the theoretical study

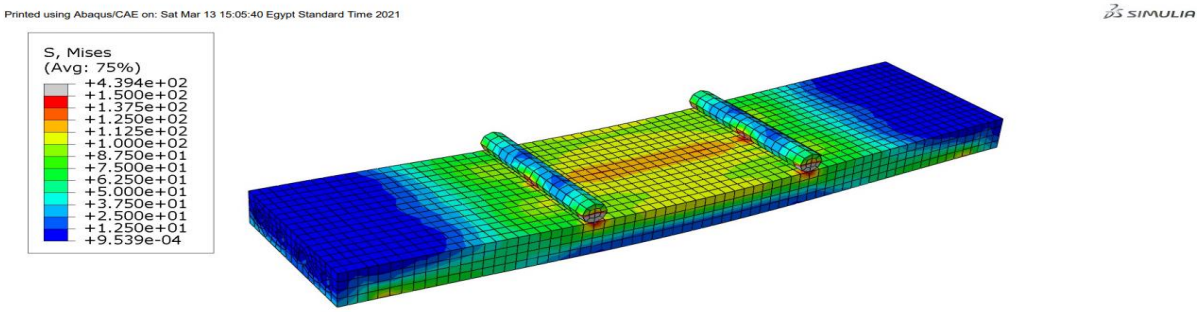

m) Stress distribution for panel T2 from the theoretical study

Fig. 30. Stress distribution for all tested specimens from the theoretical study.

Acknowledgements

None declared.

Funding

The authors received no financial support for the research, authorship, and/or publication of this manuscript.

Conflict of Interest

The authors declared no potential conflicts of interest with respect to the research, authorship, and/or publication of this manuscript.

References

Abbass AA, Abid SR, Arna'ot FH, Al-Ameri R A, Özakça M (2020). Flexural response of hollow high strength concrete beams considering different size reductions. *Journal of Structures*, 23, 69-86.

Abdul-Fataha S (2014). Structural behavior of concrete beams reinforced with innovative materials. *M.Sc. thesis*, Department of Civil Engineering, Menoufia University, Egypt.

Aboul-Anen B, El-Shafey A, El-Shami M (2009). Experimental and analytical model of ferrocement slabs. *International Journal of Recent Trends in Engineering*, 1(6), 25-29.

ACI 549 (1999) .State-of-the-Art Report on Ferrocement. ACI Manual of Concrete Practice, Part 5.

Acma L, Dumpasan G, Salva M, Mansaguiton M, Supremo R, Daquiado N (2015). Flexural strength and ductility behavior of ferrocement I-beam. *Mindanao Journal of Science and Technology*, 13, 99-108.

Al-Kubaisy MA, Jumaat MZ (2000). Flexural behavior of reinforced concrete slabs with ferrocement tension zone cover. *Construction and Building Materials*, 14(5), 245-252.

Ali A, Abdullah A (1995). Applications of ferrocement as a low cost construction material in Malaysia. *Journal of Ferrocement*, 25(2), 123-128.

ASTM C1116/C1116M-10a (2015). Standard specification for fiber reinforced concrete. ASTM international, West Conshohocken, PA.

Bhalsing S, Shoaib S, Autade P (2014). Tensile strength of ferrocement with respect to specifc surface. International *Journal of Innovative Research in Science, Engineering and Technology*, 3(4), 501-507.

Chowdary PA (2016). Experimental analytical and investigation of flexural behavior of reinforced concrete beam. *International Journal of Advanced Scientific Technology in Engineering and Management Sciences*, 2(12).

Du W, Yang C, Wang C, Pan Y, Zhang H, Yuan W (2021). Flexural behavior of polyvinyl alcohol fiber - reinforced ferrocement cementitious composite. *Journal of Materials in Civil Engineering*, 33(4).

E.C.P. 203 (2018). Egyptian Code of Practice: Design and Construction for Reinforced Concrete Structures. Cairo, Egypt.

Elavenil S, Chandrasekar V (2007). Analysis of reinforced concrete beams strengthened with ferrocement. *International Journal of Applied Engineering Research*, 2(3), 431- 440.

Eskandari H, Madadi A (2015). Investigation of ferrocement channels using experimental and finite element analysis. *Engineering Science and Technology, an International Journal*, 18(4), 769-775.

E.S.S. 1109 (2008). Aggregates for Concrete. Egyptian Organization for Standardization & Quality, Cairo, Egypt.

E.S.S. 4756-1 (2013). Portland Cement, Ordinary and Rapid Hardening. Egyptian Organization for Standardization & Quality, Cairo, Egypt.

Fahmy EH, Shaheen YB, Korany YS (1997). Use of ferrocement laminates for repairing reinforced concrete slabs. *Journal of Ferrocement*, 27(3), 219-232.

Fahmy EH, Ezzat H, Shaheen YB, Abou Zeid MN (2004). Development of ferrocement panels for floor and wall construction. *Proceedings of the 5th Structural Specialty Conference of the Canadian Society for Civil Engineering*, Saskatoon, Saskatchewan, Canada.

Fahmy EH, Ezzat H, Shaheen YB, Abou Zeid MN, Abdel Naby AM (2005). Permanent ferrocement forms: a viable alternative for construction

of concrete Beams. Proce*edings of the 30th Conference on Our World in Concrete and Structures*, Singapore, 249-256.

Koukousel A, Mistakid E (2014). Buckling behavior of composite ferrocement plates. *Conference: 8th Hellenic National Conference of Steel Structures*.

Leeanansaksiri A, Payakapo P, Ruangrassamee A (2018). Seismic capacity of masonry infilled RC frame strengthening with expanded metal ferrocement. *Journal of Engineering Structures*, 159, 110-127.

Naaman AE (2015). Ferrocement: Progress review and most critical need for the near future. *11th International Symposium on Ferrocement and Textile Reinforced Concrete 3rd ICTRC*, Germany, 9-14.

Naser FH, Al Mamoori AH, Dhahir MK (2021). Effect of using different types of reinforcement on the flexural behavior of ferrocement hollow core slabs embedding PVC pipes. *Ain Shams Engineering Journal*, 12(1), 303-315.

Prakashan LV, George J, Edayadiyil JB, George JM (2016). Experimental study on the flexural behavior of hollow core concrete slabs. *Journal of Applied Mechanics and Materials*, 857, 107-112.

Sakthivel PB, Jagannathan A (2005). Ferrocement construction technology and its applications – A review. http://dl.lib.mrt.ac.lk/handle/123/9492.

Shaaban IG, Shaheen YB, Elsayed EL, Kamal OA, Adesina PA (2018). Flexural behaviour and theoretical prediction of lightweight ferrocement composite beams. *Case Studies in Construction Materials*, 9.

Shaheen YB, Eltehawy EA (2017). Structural behaviour of ferrocement channels slabs for low cost housing. *Challenge Journal of Concrete Research Letters*, 8(2), 48-64.

Shaheen YB, Eltaly BE, Abdul-Fataha S (2014a). Structural performance of ferrocement beams reinforced with composite materials. *Journal of Structural Engineering & Mechanics*, 50(6), 817-834.

Shaheen YB, Eltaly BE, Hanesh AA (2014b). Experimental and FE simulations of ferrocement domes reinforced with composite materials. *Journal of Concrete Research Letters*, 5(4), 873-887.

Shaheen YB, Nasser AA, El-Habashy WS (2016). Behaviour of ferrocement sandwich panels slabs under shear. *Journal of Concrete Research Letters*, 7(1), 11-23.

Shaheen YB, Soliman NM, El-Araby F (2018). Repairing reinforced concrete beams with openings by ferrocement laminates. *12th International Conference on Civil and Architecture Engineering*, Cairo, Egypt, 1-20.

Shaheen YB, Mousa M, Gamal E (2020). Structural behavior of light weight ferrocement walls. *13th International Conference on Civil and Architecture Engineering*, Cairo, Egypt, 1-21.

Singh V, Bansal PP, Kumar M (2015). Experimental studies on strength and ductility of ferrocement jacketed RC beam-column joints. *International Journal of Civil and Structural Engineering*, 5(3), 199-205.

Swamy RN, Shaheen YB (1990). Tensile behavior of thin ferrocement plates. *ACI Materials Journal*, 357-387.